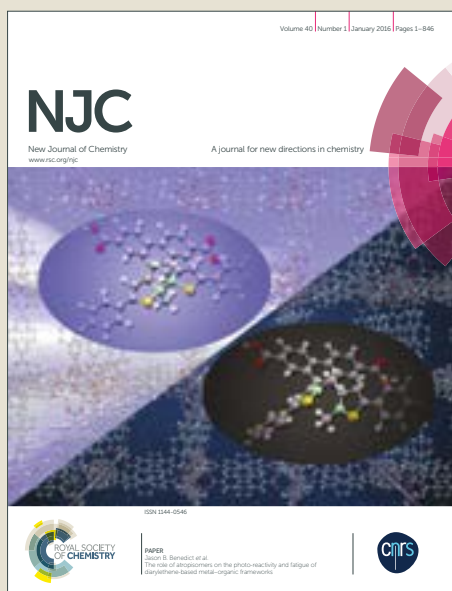


NJC

Accepted Manuscript



This article can be cited before page numbers have been issued, to do this please use: S. A. Patil, V. Kandathil, B. Fahlman, S. B. S and S. Patil, *New J. Chem.*, 2017, DOI: 10.1039/C7NJ01876B.



This is an Accepted Manuscript, which has been through the Royal Society of Chemistry peer review process and has been accepted for publication.

Accepted Manuscripts are published online shortly after acceptance, before technical editing, formatting and proof reading. Using this free service, authors can make their results available to the community, in citable form, before we publish the edited article. We will replace this Accepted Manuscript with the edited and formatted Advance Article as soon as it is available.

You can find more information about Accepted Manuscripts in the [author guidelines](#).

Please note that technical editing may introduce minor changes to the text and/or graphics, which may alter content. The journal's standard [Terms & Conditions](#) and the ethical guidelines, outlined in our [author and reviewer resource centre](#), still apply. In no event shall the Royal Society of Chemistry be held responsible for any errors or omissions in this Accepted Manuscript or any consequences arising from the use of any information it contains.

A Convenient, Efficient and Reusable N-Heterocyclic Carbene–Palladium(II) Based Catalyst Supported on Magnetite for Suzuki–Miyaura and Mizoroki–Heck Cross-Coupling Reactions

Vishal Kandathil,^a Bradley D. Fahlman,^b Sasidhar B. S.,^c Shivaputra A. Patil,^d Siddappa A. Patil^{a*}

^aCentre for Nano and Material Sciences, Jain University, Jain Global Campus, Kanakapura, Ramanagaram, Bangalore 562112, India.

^bDepartment of Chemistry and Biochemistry & Science of Advanced Materials, Central Michigan University, Mount Pleasant, MI 48859, USA.

^cOrganic Chemistry Section, Chemical Sciences and Technology Division, CSIR-National Institute for Interdisciplinary Science and Technology, Thiruvananthapuram-695019, India.

^dPharmaceutical Sciences Department, College of Pharmacy, Rosalind Franklin University of Medicine and Science, North Chicago, IL 60064 USA.

Corresponding author: Dr. Siddappa A. Patil

Tel: +91 80 27577254

Fax: +91 80 27577211

E-mail: p.siddappa@jainuniversity.ac.in

Abstract

In the present work, a new magnetic nanoparticle supported N-heterocyclic carbene–palladium(II) ($\text{NO}_2\text{-NHC-Pd@Fe}_3\text{O}_4$) nanomagnetic catalyst was synthesized by a facile multistep synthesis under aerobic conditions using inexpensive chemicals. The $\text{NO}_2\text{-NHC-Pd@Fe}_3\text{O}_4$ nanomagnetic catalyst was characterized by various analytical techniques such as attenuated total reflectance infrared spectroscopy (ATR-IR), inductively coupled plasma-atomic emission spectroscopy (ICP-AES), energy-dispersive X-ray spectroscopy (EDS), field-emission scanning electron microscopy (FESEM), transmission electron microscopy (TEM), X-ray powder diffraction (XRD), thermogravimetric analysis (TGA) and Brunauer-Emmett-Teller surface area analysis (BET). The synthesized $\text{NO}_2\text{-NHC-Pd@Fe}_3\text{O}_4$ nanomagnetic catalyst showed excellent catalytic activity in both Suzuki-Miyaura and Mizoroki-Heck cross-coupling reactions for various substrates under mild reaction conditions. Recovery of $\text{NO}_2\text{-NHC-Pd@Fe}_3\text{O}_4$ nanomagnetic catalyst from the reaction mixture was easily accomplished by applying external magnet. The recovered $\text{NO}_2\text{-NHC-Pd@Fe}_3\text{O}_4$ nanomagnetic catalyst exhibited very good catalytic activity up to seven recycles in Suzuki-Miyaura and five recycles in Mizoroki-Heck cross-coupling reactions without considerable loss of its catalytic activity.

Keywords: Magnetic nanoparticle; N-heterocyclic carbene-palladium(II); nanomagnetic catalyst; Synthesis and characterization; Suzuki-Miyaura and Mizoroki-Heck cross-coupling reactions

1. Introduction

Carbon-carbon bond formation reactions of aryl halides with organoboronic acids in the presence of palladium and a base, the Suzuki–Miyaura cross-coupling reaction, is one of the most important and flexible reactions for the synthesis of various biaryls which constitute important structural units in various natural products, pharmaceutical intermediates, polymers and many more.¹⁻⁴ The notable advantage of using organoboronic acids is their increased stability in air and moisture, mild reaction conditions, and the feasibility of reactions with a wide range of functional groups.⁵ In addition, arylation of olefins in the presence of palladium and a base, the Mizoroki–Heck cross-coupling reaction, is an enormously useful and common strategy for synthesizing functionalized olefins⁶, which contributes a wide range of molecules of use in pharmaceutical, phytochemical, agrochemical, and polymer industries⁷. Thus, palladium catalyzed cross-coupling reactions are a very significant and powerful tool in the synthesis of numerous molecules with diverse physical, chemical and biological activities.^{8,9}

Even though palladium catalyzed cross-coupling reactions are very important, the commercial production of such cross-coupled products are expensive because of the precious noble metal palladium. As a result, recovery and reuse of the precious palladium based catalyst will help to reduce the cost of production minimize palladium poisoning in the active pharmaceutical intermediates, and reduce waste generation.¹⁰ To improve their recyclability, homogeneous catalysts are typically grafted onto different types of supports, rendering them heterogeneous in nature.¹¹⁻¹³ By implementing a magnetic support to a homogeneous catalyst makes it easily recyclable with the help of an external magnet, thereby avoiding filtration or centrifugation techniques for recovery of the catalyst.¹³⁻¹⁶

Phosphine ligands are widely employed in palladium catalyzed cross-coupling reactions.^{17, 18} However, these ligands have some shortcomings like air and moisture sensitivity, and they are also toxic in nature.¹⁹ The isolation of stable *N*-heterocyclic carbenes (NHCs) in 1991 by Arduengo²⁰, and subsequent research on NHCs, has revealed that they are good substitutes for phosphines as ligands in catalysis.²¹⁻²³ The chief advantages of NHCs over phosphines are their comparable or superior activity, higher dissociation energy, ease of large-scale synthesis, less toxicity, and increased stability in air and moisture.^{24, 25} The use of NHC ligands has many advantages over phosphine analogs in many palladium catalyzed cross-coupling reactions such as Suzuki–Miyaura, Mizoroki–Heck, Buchwald–Hartwig and Sonogashira cross-coupling reactions.^{24, 26, 27} The strong σ -donor capability of NHC ligand facilitates the oxidative addition step in the catalytic cycle of cross-coupling reactions.^{25, 28-32} Also, reductive elimination in the last step of catalytic cycle is promoted by the increased steric bulk around the metal in the NHC.²⁸ The metal-leaching issue is less pronounced in the case of NHC–metal complexes, which is due to the strong carbene-metal bond they form; for these reasons, these complexes also possess high thermal stability.²²

Thus, in continuation of our previous work³³, which is focused on green and sustainable pathways in the field of catalysis and the search for new potential catalysts, we report herein the synthesis, characterization and catalytic activity of a new NO₂-NHC-Pd@Fe₃O₄, nanomagnetic catalyst for Suzuki–Miyaura and Mizoroki–Heck cross-coupling reactions. The prepared NO₂-NHC-Pd@Fe₃O₄ nanomagnetic catalyst is stable under air and moisture and can be synthesized easily from commercially available inexpensive chemicals. The NO₂-NHC-Pd@Fe₃O₄ nanomagnetic catalyst exhibited excellent catalytic activity in both Suzuki–Miyaura and Mizoroki–Heck cross-coupling reactions with good recyclability. The better catalytic activity of

NO₂-NHC-Pd@Fe₃O₄ nanomagnetic catalyst in Suzuki–Miyaura and Mizoroki–Heck cross-coupling reactions may be due to the increased steric bulk caused by the addition of nitro group on the phenyl ring in the present NHC ligand as compared to previously reported NHC-Pd@MNPs nanomagnetic catalyst from our laboratory.³³

2. Experimental

2.1 Materials

Unless otherwise stated, all reactions were performed under aerobic conditions in oven-dried glassware with magnetic stirring. FeCl₃·6H₂O, FeCl₂·4H₂O, sodium carbonate, cesium carbonate, potassium carbonate, ammonium hydroxide, 4-nitrobenzyl bromide, benzimidazole, (3-chloropropyl)triethoxysilane, palladium(II) acetate, aryl halides, phenylboronic acid, styrene, *tert*-butyl acrylate, sodium phosphate tribasic dodecahydrate, were purchased from Sigma-Aldrich chemical company and were used without further purification. Solvents were dried and degassed using a JC Meyer company solvent purification system. Heating was accomplished by either a heating mantle or silicone oil bath. Reactions were monitored by thin-layer chromatography (TLC) performed on 0.25 mm Merck TLC silica gel plates, using UV light as a visualizing agent. Purification of reaction products was carried out by flash column chromatography using silica gel 60 (230–400 mesh). Yields refer to chromatographically pure material. Concentration *in vacuo* refers to the removal of volatile solvent using a rotary evaporator attached to a dry diaphragm pump (10–15 mm Hg), followed by pumping to a constant weight with an oil pump (< 300 mTorr).

2.2 Characterization

Attenuated total reflectance infrared spectra were recorded with a Bruker Alpha Eco-ATR spectrometer. Brunauer-Emmett-Teller surface areas were obtained by physisorption of N₂

using a Microtrac BELSORP MAX instrument. The elemental palladium content of the NO₂-NHC-Pd@Fe₃O₄ nanomagnetic catalyst was determined by Thermo Electron IRIS INTREPID II XSP DUO inductively coupled plasma atomic emission spectroscopy. Transmission electron microscope images were obtained using Jeol/JEM 2100 microscope. A JEOL JSM 7100F field-emission scanning electron microscope (FESEM), fitted with energy dispersive X-ray spectroscopy, was used to observe the morphology and elemental distributions of samples. Thermogravimetric analysis was carried out using a Perkin Elmer, Diamond TG/DTA with a heating rate of 10.0 °C/min. X-ray powder diffraction patterns were obtained using a Bruker AXS D8 Advance diffractometer. ¹H NMR spectra were recorded at 400 MHz, and are reported relative to CDCl₃ (δ 7.27). ¹H NMR coupling constants (*J*) are reported in Hertz (Hz) and multiplicities are indicated as follows: s (singlet), d (doublet), t (triplet), and m (multiplet). Liquid chromatography mass spectra (LC-MS) were recorded on an Agilent technologies quadrupole LC-MS system. The single-crystal X-ray diffraction data was collected on a Bruker AXS Kappa Apex 2 CCD diffractometer at 293(2) K. Crystallographic data of the structure reported in this article was deposited to the Cambridge Crystallographic Data Center with the deposition number 1552582. A copy of the data can be obtained free of charge from the Director, CCDC, 12 Union Road, Cambridge CB2 1EZ, UK [fax: +44 1223 336-033; e-mail: deposit@ccdc.cam.ac.uk or www.ccdc.cam.ac.uk/deposit]

2.3 Synthesis of magnetite (Fe₃O₄, magnetic nanoparticles)

Magnetic nanoparticles (MNPs) were synthesized through a co-precipitation method, as described in our previous work.³³ Briefly, FeCl₃·6H₂O (2.35g, 8.7 mmol) and FeCl₂·4H₂O (0.86 g, 4.3 mmol) were dissolved in deionized water (40 mL). The reaction mixture was then stirred at 85 °C for 30 minutes to completely dissolve both the reactants. Ammonium hydroxide (5 mL)

solution was then added slowly to the reaction mixture with vigorous stirring at 85 °C to generate a black colored precipitate. The reaction was continued for an additional 30 minutes. The precipitated magnetic nanoparticles were then isolated by magnetic decantation, washed with deionized water repeatedly until neutral pH, further washed with ethanol (2 x 20 mL), and dried at 80 °C for 6 h.

2.4 Synthesis of silyl chloride functionalized magnetic nanoparticles (SMNPs)

In an ethanol:water (EtOH:H₂O) (1:1) mixture (20 mL), hydroxyl-substituted magnetic nanoparticles (2.0 g) were dispersed by ultrasonication for 30 minutes, followed by the addition of (3-chloropropyl)triethoxysilane (2.0 g, 8.3 mmol). Then, the reaction mixture was stirred at 45 °C for 24 h. The precipitated dark brown colored silyl chloride-functionalized magnetic nanoparticles were isolated by magnetic decantation after cooling to room temperature, washed with deionized water (2 x 20 mL) and ethanol (2 x 20 mL) and dried at 60 °C *in vacuo*.

2.5 Synthesis of 1-(4-nitrobenzyl)-1H-benzimidazole

The synthesis of 1-(4-nitrobenzyl)-1H-benzimidazole was carried out according to a published literature procedure with slight modification.³⁴ Benzimidazole (1.0 g, 8.46 mmol) was added to a round-bottomed flask containing methanol (20 mL). The reaction mixture was stirred at room temperature for 10 minutes. Cesium carbonate was then added into the reaction mixture under stirring, followed by cooling the reaction mixture to 5-10 °C. After 10 minutes, 4-nitrobenzyl bromide was added under stirring at the same temperature. After 15 minutes, the temperature was raised to room temperature, with continued stirring of the reaction mixture. The progress of the reaction was monitored by TLC using ethyl acetate-hexane as an eluent. After reaction completion, the reaction mixture was added to water (60 mL) with stirring to precipitate the product as a yellow-colored solid. The solid was filtered and washed with water (2 x 40 mL),

and dried at 50 °C *in vacuo* to yield 1-(4-nitrobenzyl)-1*H*-benzimidazole as a yellow-colored solid. Yield: 90%; Melting point = 83-86 °C; ¹H NMR (400 MHz, CDCl₃): δ (ppm) = 8.17 (d, *J* = 8.0 Hz, 2H), 7.96 (s, 1H, NCHN), 7.41-7.38 (m, 4H), 7.32-7.29 (m, 2H), 5.25 (s, 2H, CH₂C₆H₅).

2.6 Synthesis of magnetic nanoparticle-tethered 1-(4-nitrobenzyl)-1*H*-benzimidazolium chloride (NO₂-NHC@Fe₃O₄)

In toluene (40 mL), silyl chloride-functionalized magnetic nanoparticles (2.0 g) were suspended by ultrasonication for 30 minutes. 1-(4-Nitrobenzyl)-1*H*-benzimidazole (1.0 g, 4.8 mmol) was added in one portion to the reaction mixture and stirred at 110 °C for 48 h. The reaction mixture was then cooled to room temperature. The resulted brown colored solid was isolated by magnetic decantation, washed with toluene (5 x 20 mL) and dried at 50 °C under reduced pressure for 12 h to yield a brown-coloured solid, NO₂-NHC@Fe₃O₄.

2.7 Synthesis of magnetic nanoparticle supported *N*-heterocyclic carbene-palladium(II) complex (NO₂-NHC-Pd@Fe₃O₄)

To a solution of Na₂CO₃ (0.5 M, 20 mL) in dimethylformamide (DMF) (20 mL), palladium(II) acetate (0.22 g, 0.98 mmol) was added and the reaction mixture was stirred at room temperature for 15 minutes. Magnetic nanoparticle-tethered 1-(4-nitrobenzyl)-1*H*-benzimidazolium chloride (1.0 g) was then added to the reaction mixture and stirred at 50 °C for 16 h. Then, the reaction mixture was cooled to room temperature. The resultant product was isolated by magnetic decantation, washed with water (2 x 20 mL) and methanol (2 x 20 mL), and dried under reduced pressure for 6 h at 45 °C to yield a brown-coloured solid, the NO₂-NHC-Pd@Fe₃O₄ nanomagnetic catalyst.

2.8 General procedure for Suzuki-Miyaura cross-coupling reactions

The magnetic nanoparticle supported NHC-palladium(II) complex ($\text{NO}_2\text{-NHC-Pd@Fe}_3\text{O}_4$, nanomagnetic catalyst) (0.15 mol% Pd), aryl halide (1.0 mmol), phenylboronic acid (1.1 mmol) and potassium carbonate (2.2 mmol) were placed in a round-bottomed flask. To the reaction mixture, EtOH:H₂O (1:1, 5 mL) was added and stirred at room temperature for designated hours. The progress of the reaction was monitored by TLC. After reaction completion, the $\text{NO}_2\text{-NHC-Pd@Fe}_3\text{O}_4$ nanomagnetic catalyst was separated by using an external magnet. To the reaction mixture, ethyl acetate (10 mL) and water (10 mL) were added. The cross-coupled product was extracted to ethyl acetate from water using a separatory funnel and dried with magnesium sulphate. The dried ethyl acetate was concentrated *in vacuo*, and the product was purified by column chromatography using *n*-hexane and ethyl acetate as eluents to afford the corresponding products in good to excellent yields. All the cross-coupling products were known molecules and were confirmed by comparing the melting point, ¹H NMR and mass spectroscopic data with authentic samples.

1. *Biphenyl* (Table 2, entries 1, 2 and 3): Colorless crystals. Melting point = 68-70 °C; ¹H NMR (400 MHz, CDCl₃): δ (ppm) = 7.35 (t, *J* = 7.6 Hz, 2H), 7.42 (t, *J* = 7.6 Hz, 4H), 7.6 (d, *J* = 8.0 Hz, 4H). LC-MS for C₁₂H₁₀: *m/z* = 155.07 [M+H]⁺.

2. *4-Methylbiphenyl* (Table 2, entries 4 and 5): White crystalline solid. Melting point = 45-47 °C; ¹H NMR (400 MHz, CDCl₃): δ (ppm) = 7.57 (d, *J* = 6.0 Hz, 2H), 7.49 (d, *J* = 6.0 Hz, 2H), 7.42 (d, *J* = 6.0 Hz, 2H), 7.30 (t, *J* = 6.0 Hz, 1H), 7.24 (d, *J* = 6.0 Hz, 2H), 2.38 (s, 3H). LC-MS for C₁₃H₁₂: *m/z* = 169.05 [M+H]⁺.

3. *4-Acetylbiphenyl* (Table 2, entries 6 and 7): White powder. Melting point = 119-123 °C; ¹H NMR (400 MHz, CDCl₃): δ (ppm) = 8.03 (d, *J* = 8.0 Hz, 2H), 7.69 (d, *J* = 8.0 Hz, 2H), 7.63 (d, *J* = 7.6 Hz, 2H), 7.45-7.48 (m, 2H), 7.39-7.37 (m, 1H), 2.63 (s, 3H). LC-MS for C₁₄H₁₂O: *m/z* = 197.17 [M+H]⁺.

4. *4-Hydroxybiphenyl* (Table 2, entries 8, 9 and 10): White crystals. Melting point = 164-166 °C; ¹H NMR (400 MHz, CDCl₃): δ (ppm) = 7.51 (d, *J* = 7.2 Hz, 2H), 7.47 (d, *J* = 7.2 Hz, 2H), 7.36 (d, *J* = 8.0 Hz, 2H), 7.30-7.28 (m, 1H), 6.89 (d, *J* = 8.0 Hz, 2H), 4.81 (s, 1H). LC-MS for C₁₂H₁₀O: *m/z* = 171.15 [M+H]⁺.

5. *4-Cyanobiphenyl* (Table 2, entry 11): Off-white crystalline powder. Melting point = 85-87 °C; ^1H NMR (400 MHz, CDCl_3): δ (ppm) = 7.73-7.65 (m, 4H), 7.59 (d, J = 8.0 Hz, 2H), 7.50-7.47 (t, J = 8.0 Hz, 2H), 7.43-7.41 (m, 1H). LC-MS for $\text{C}_{13}\text{H}_9\text{N}$: m/z = 180.01 $[\text{M}+\text{H}]^+$.

6. *4-Nitrobiphenyl* (Table 2, entry 12): Pale yellow crystals. Melting point = 112-114 °C; ^1H NMR (400 MHz, CDCl_3): δ (ppm) = 8.28 (d, J = 8.0 Hz, 2H), 7.72 (d, J = 8.0 Hz, 2H), 7.61 (d, J = 8.0 Hz, 2H), 7.50-7.44 (m, 3H). LC-MS for $\text{C}_{12}\text{H}_9\text{NO}_2$: m/z = 200.04 $[\text{M}+\text{H}]^+$.

7. *4-Aminobiphenyl* (Table 2, entry 13): Purple crystals. Melting point = 52-55 °C; ^1H NMR (400 MHz, CDCl_3): δ (ppm) = 7.54 (d, J = 8.4 Hz, 2H), 7.44-7.41 (m, 4H), 7.28-7.24 (m, 1H), 6.78 (d, J = 8.0 Hz, 2H), 3.72 (s, 2H). LC-MS for $\text{C}_{12}\text{H}_{11}\text{N}$: m/z = 170.03 $[\text{M}+\text{H}]^+$.

8. *4-Phenylbenzaldehyde* (Table 2, entry 14): Yellow crystals. Melting point = 57-59 °C; ^1H NMR (400 MHz, CDCl_3): δ (ppm) = 9.98 (s, 1H), 7.88 (d, J = 6.4 Hz, 2H), 7.68 (d, J = 6.0 Hz, 2H), 7.57 (d, J = 6.8 Hz, 2H), 7.42 (m, 3H). LC-MS for $\text{C}_{13}\text{H}_{10}\text{O}$: m/z = 183.09 $[\text{M}+\text{H}]^+$.

9. *2-Phenylbenzaldehyde* (Table 2, entries 15 and 16): Yellow oil. ^1H NMR (400 MHz, CDCl_3): δ (ppm) = 9.98 (s, 1H), 8.01 (d, J = 6.0 Hz, 1H), 7.63 (t, J = 6.0 Hz, 1H), 7.47 (m, 5H), 7.38 (d, J = 6.0 Hz, 2H). LC-MS for $\text{C}_{13}\text{H}_{10}\text{O}$: m/z = 183.05 $[\text{M}+\text{H}]^+$.

10. *4-Phenylbenzoic acid* (Table 2, entry 17): White solid. Melting point = 219-224 °C; ^1H NMR (400 MHz, CDCl_3): δ (ppm) = 8.03 (d, J = 6.0 Hz, 2H), 7.81 (d, J = 6.0 Hz, 2H), 7.74 (d, J = 6.0 Hz, 2H), 7.52-7.49 (t, J = 6.0 Hz, 2H), 7.44-7.41 (t, J = 6.4 Hz, 1H). LC-MS for $\text{C}_{13}\text{H}_{10}\text{O}_2$: m/z = 199.11 $[\text{M}+\text{H}]^+$.

11. *3-Phenylbenzoic acid* (Table 2, entry 18): Off-white crystals. Melting point = 164-168 °C; ^1H NMR (400 MHz, CDCl_3): δ (ppm) = 8.18 (s, 1H), 7.93 (t, J = 7.2 Hz, 2H), 7.70 (d, J = 6.0 Hz, 2H), 7.61 (t, J = 7.2 Hz, 1H), 7.52-7.40 (m, 3H). LC-MS for $\text{C}_{13}\text{H}_{10}\text{O}_2$: m/z = 199.06 $[\text{M}+\text{H}]^+$.

12. *4-Methoxybiphenyl* (Table 2, entries 19 and 20): White powder. Melting point = 86-90 °C; ^1H NMR (400 MHz, CDCl_3): δ (ppm) = 7.54-7.51 (m, 4H), 7.40 (t, J = 7.2 Hz, 2H), 7.30 (t, J = 7.6 Hz, 1H), 6.98 (d, J = 8.0 Hz, 2H), 3.85 (s, 3H). LC-MS for $\text{C}_{13}\text{H}_{12}\text{O}$: m/z = 185.10 $[\text{M}+\text{H}]^+$.

13. *2,4-Difluoro-1,1'-biphenyl* (Table 2, entry 21): Pale yellow crystals. Melting point = 61-65 °C; ^1H NMR (400 MHz, CDCl_3): δ (ppm) = 7.58 (d, J = 6.0 Hz, 1H), 7.48 (d, J = 6.0 Hz, 2H), 7.42-7.36 (m, 4H), 6.91-6.89 (m, 1H). LC-MS for $\text{C}_{12}\text{H}_8\text{F}_2$: m/z = 191.02 $[\text{M}+\text{H}]^+$.

2.9 General procedure for Mizoroki-Heck cross-coupling reactions

The magnetic nanoparticle supported NHC-palladium(II) complex ($\text{NO}_2\text{-NHC-Pd@Fe}_3\text{O}_4$, nanomagnetic catalyst) (1.0 mol% Pd), aryl halide (1.0 mmol), alkene (1.2 mmol) and sodium phosphate tribasic dodecahydrate (2.0 mmol) were placed in a round-bottomed flask. To the reaction mixture, acetonitrile (5 mL) was added and stirred at 80 °C for designated hours. The progress of the reaction was monitored by TLC. After reaction completion, the reaction

mixture to room temperature, and the NO₂-NHC-Pd@Fe₃O₄ nanomagnetic catalyst was separated by using an external magnet. To the reaction mixture, ethyl acetate (10 mL) and water (10 mL) were added. The ethyl acetate layer was separated from water layer through separatory funnel and dried with magnesium sulphate. The dried ethyl acetate was concentrated *in vacuo*, and the product was purified by column chromatography using *n*-hexane and ethyl acetate as eluents to afford the corresponding products in moderate to excellent yields. All the coupling products were known molecules and were confirmed by comparing the ¹H NMR spectral data with the authentic samples.

1. (*E*)-1,2-diphenylethene (Table 5, entries 1 and 2): White solid; ¹H NMR (400 MHz, CDCl₃): δ (ppm) = 7.53-7.51 (m, 4H), 7.36 (t, *J* = 8.0 Hz, 4H), 7.28-7.24 (m, 4H).

2. (*E*)-*tert*-butyl 3-(4-hydroxyphenyl)acrylate (Table 5, entries 3, 4 and 5): Light brown liquid; ¹H NMR (400 MHz, CDCl₃): δ (ppm) = 7.53 (d, *J* = 15.8 Hz, 1H), 7.40 (s, 2H), 6.83 (s, 2H), 6.24 (d, *J* = 15.8 Hz, 1H), 1.53 (s, 9H).

3. (*E*)-*tert*-butyl 3-(*p*-tolyl)acrylate (Table 5, entries 6 and 7): Light yellow liquid; ¹H NMR (400 MHz, CDCl₃): δ (ppm) = 7.40 (d, *J* = 8.0 Hz, 3H), 7.29 (s, 2H), 6.27 (d, 16.0 Hz, 1H), 2.29 (s, 3H), 1.53 (s, 9H).

4. (*E*)-1-methyl-4-styrylbenzene (Table 5, entries 8 and 9): White solid; ¹H NMR (400 MHz, CDCl₃): δ (ppm) = 7.88 (s, 2H), 7.64-7.39 (m, 9H), 2.18 (s, 3H).

5. (*E*)-*tert*-butyl 3-(4-acetylphenyl)acrylate (Table 5, entries 10 and 11): Yellow liquid; ¹H NMR (400 MHz, CDCl₃): δ (ppm) = 7.33-7.05 (m, 5H), 6.11 (d, *J* = 16.0 Hz, 1H), 2.25 (s, 3H), 1.25 (s, 9H).

6. (*E*)-*tert*-butyl 3-(2,4-difluorophenyl)acrylate (Table 5, entry 12): Light brown liquid; ¹H NMR (400 MHz, CDCl₃): δ (ppm) = 7.72 (d, *J* = 15.8 Hz, 1H), 7.54 (d, *J* = 8.0 Hz, 3H), 7.37 (d, *J* = 15.8 Hz, 1H), 1.28 (s, 9H).

7. (*E*)-*tert*-butyl 3-(4-cyanophenyl)acrylate (Table 5, entries 13 and 14): Colorless crystal; ¹H NMR (400 MHz, CDCl₃): δ (ppm) = 7.84 (d, *J* = 8.0 Hz, 3H), 7.70 (d, *J* = 8.0 Hz, 2H), 6.64 (d, *J* = 16.0 Hz, 1H), 1.53 (s, 9H).

8. *tert*-butyl cinnamate (Table 5, entry 15): Off-white solid; ¹H NMR (400 MHz, CDCl₃): δ (ppm) = 7.56 (d, *J* = 15.8 Hz, 1H), 7.51 (s, 2H), 7.36 (d, *J* = 8.0 Hz, 3H), 6.37 (d, *J* = 16.0 Hz, 1H), 1.53 (s, 9H).

9. (*E*)-*tert*-butyl 3-(4-methoxyphenyl)acrylate (Table 5, entries 16, 17 and 18): Yellow liquid; ^1H NMR (400 MHz, CDCl_3): δ (ppm) = 7.62 (d, J = 15.8 Hz, 1H), 7.45 (s, 2H), 7.13 (d, J = 8.0 Hz, 2H), 6.24 (d, J = 16.0 Hz, 1H), 3.82 (s, 3H), 1.52 (s, 9H).

2.10 Procedure for recovery of the $\text{NO}_2\text{-NHC-Pd@Fe}_3\text{O}_4$ nanomagnetic catalyst

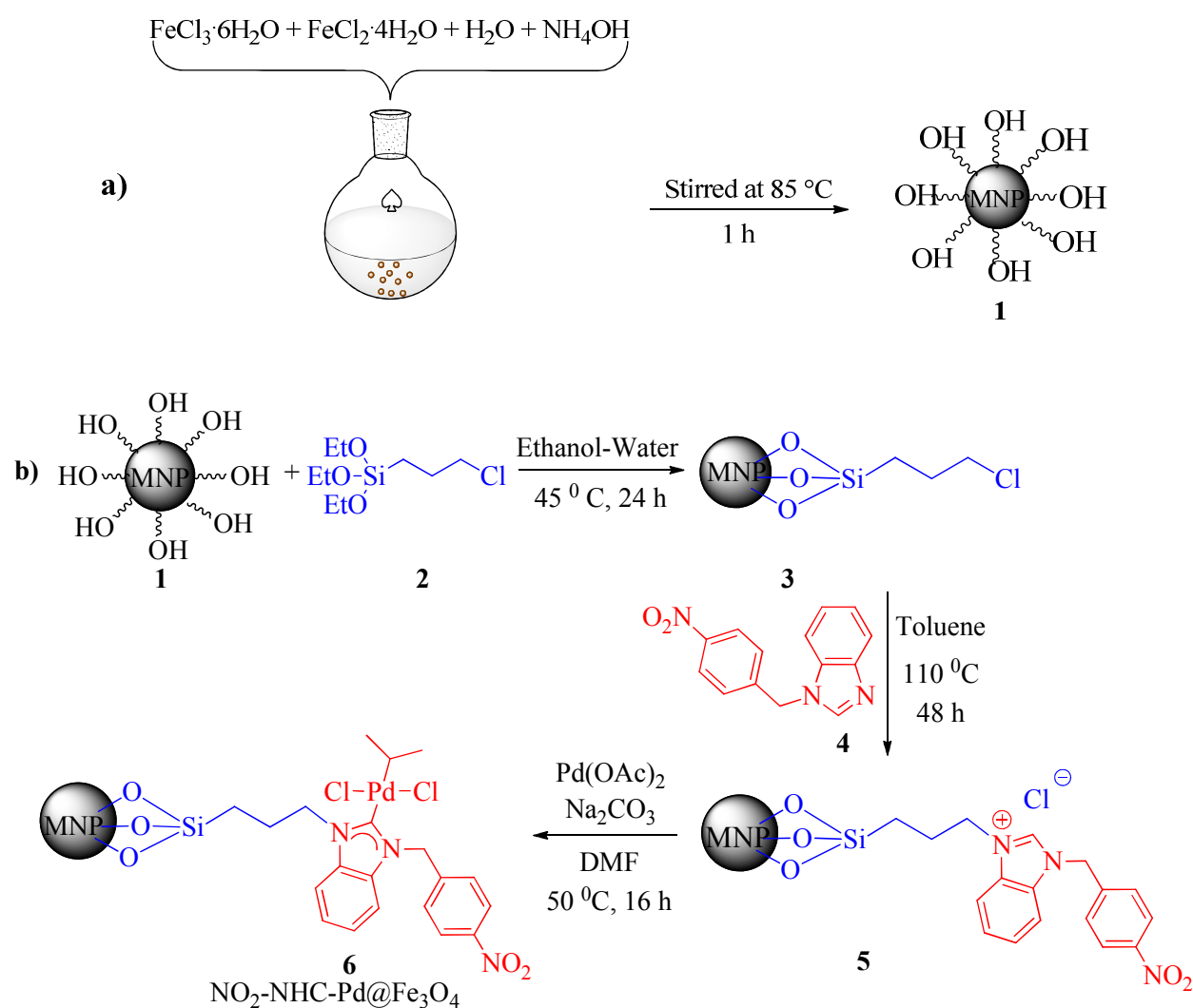
After reaction completion, the $\text{NO}_2\text{-NHC-Pd@Fe}_3\text{O}_4$ nanomagnetic catalyst was separated using an external magnet. The $\text{NO}_2\text{-NHC-Pd@Fe}_3\text{O}_4$ nanomagnetic catalyst was then subjected to washing with ethanol (2 x 10 mL), water (2 x 10 mL), and methanol (2 x 10 mL). The isolated $\text{NO}_2\text{-NHC-Pd@Fe}_3\text{O}_4$ nanomagnetic catalyst was dried at 45 °C under vacuum for 6 h. The dried $\text{NO}_2\text{-NHC-Pd@Fe}_3\text{O}_4$ nanomagnetic catalyst was used for the next round of reaction without further purification.

3. Results and Discussion

3.1 Synthesis of $\text{NO}_2\text{-NHC-Pd@Fe}_3\text{O}_4$ nanomagnetic catalyst

In an extension of our previous, the $\text{NO}_2\text{-NHC-Pd@Fe}_3\text{O}_4$ nanomagnetic catalyst was synthesized through a multistep strategy as described in Scheme 1. Hydroxyl-substituted magnetic nanoparticles (**1**) were prepared by a co-precipitation method, followed by the functionalization of magnetic nanoparticles with (3-chloropropyl)triethoxysilane (**2**) in EtOH:H₂O mixture at 45 °C. 4-Nitrobenzyl bromide was reacted with benzimidazole in the presence of cesium carbonate in methanol to get the intermediate 1-(4-nitrobenzyl)-1*H*-benzimidazole (**4**). Additionally, the structure of 1-(4-nitrobenzyl)-1*H*-benzimidazole was confirmed by single-crystal X-ray diffraction analysis. Suitable single crystals for X-ray diffraction analysis of 1-(4-nitrobenzyl)-1*H*-benzimidazole were grown by a slow evaporation method. The molecular structures of the two independent molecules (A and B) of the 1-(4-nitrobenzyl)-1*H*-benzimidazole (**4**) compound are illustrated in Fig. 1. 1-(4-Nitrobenzyl)-1*H*-benzimidazole was then treated with silyl functionalized magnetic nanoparticles (SMNPs) (**3**) in

toluene at 110 °C for 48 h. The obtained magnetic nanoparticle-tethered 1-(4-nitrobenzyl)-1*H*-benzimidazolium chloride (**5**) was treated with palladium(II) acetate in dimethylformamide (DMF) in the presence of aqueous sodium carbonate to yield the NO₂-NHC-Pd@Fe₃O₄ nanomagnetic catalyst (**6**).



Scheme 1. Synthetic schemes of (a) magnetic nanoparticles (**1**) and (b) NO₂-NHC-Pd@Fe₃O₄ nanomagnetic catalyst (**6**).

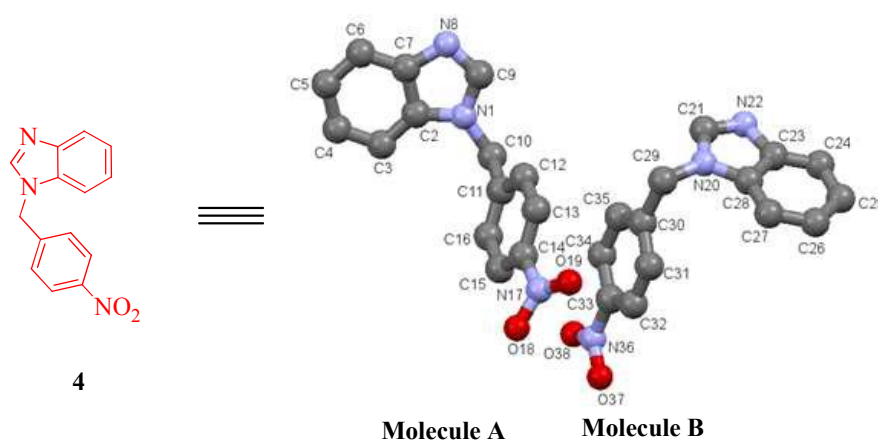


Fig. 1. A view of the molecular structure of the two independent molecules (A and B) of the 1-(4-nitrobenzyl)-1H-benzimidazole (**4**), with atom labelling. Displacement ellipsoids are drawn at the 50% probability level.

3.2 Spectroscopic and microscopic characterization of the $\text{NO}_2\text{-NHC-Pd@Fe}_3\text{O}_4$ nanomagnetic catalyst

ATR-IR was employed for the spectroscopic characterization of products formed in each step for the synthesis of the $\text{NO}_2\text{-NHC-Pd@Fe}_3\text{O}_4$ nanomagnetic catalyst. Fig. 2 shows ATR-IR spectra of Fe_3O_4 , silyl-functionalized Fe_3O_4 , and the $\text{NO}_2\text{-NHC-Pd@Fe}_3\text{O}_4$ nanomagnetic catalyst. The peaks at 585 cm^{-1} and 3392 cm^{-1} in the IR spectra of Fe_3O_4 are attributed to Fe-O and O-H stretching vibrations (Fig. 2a), respectively. The peak at 1641 cm^{-1} corresponds to the O-H overtone band, which confirms the presence of adsorbed water layer on Fe_3O_4 . Two extra peaks in Fig. 2b at 991 cm^{-1} and 2912 cm^{-1} , when compared with Fig. 2a, are due to Si-O and C-H stretching respectively, which confirms the surface functionalization of Fe_3O_4 with (3-chloropropyl)triethoxysilane. The characteristic peaks at 1521 , 1656 , and 985 cm^{-1} in the IR spectrum of the $\text{NO}_2\text{-NHC-Pd@Fe}_3\text{O}_4$ nanomagnetic catalyst (Fig. 2c) are due to N-O, C=C and Si-O vibrations, respectively, apart from the peaks at 2930 cm^{-1} and 3379 cm^{-1} , which are due to C-H and O-H stretching; this confirms the structure of the $\text{NO}_2\text{-NHC-Pd@Fe}_3\text{O}_4$ nanomagnetic

catalyst. The IR spectra of the seven-times recycled $\text{NO}_2\text{-NHC-Pd@Fe}_3\text{O}_4$ nanomagnetic catalyst shows the structure is intact even though there is some shift in the peaks, as shown in Fig. 2d.

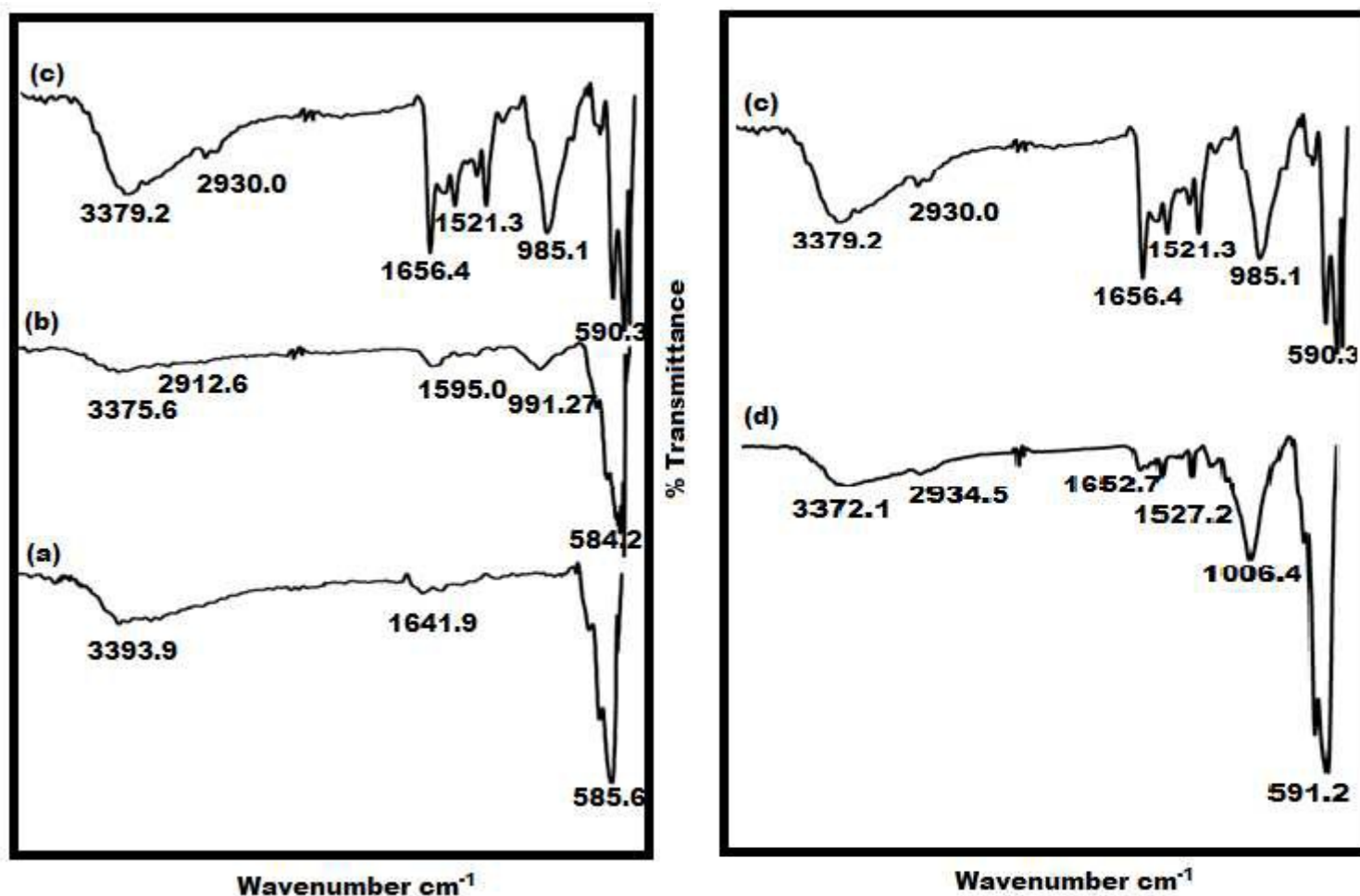


Fig. 2. ATR-IR spectra of (a) MNPs, (b) SMNPs, (c) $\text{NO}_2\text{-NHC-Pd@Fe}_3\text{O}_4$ nanomagnetic catalyst and (d) seven times recycled $\text{NO}_2\text{-NHC-Pd@Fe}_3\text{O}_4$ nanomagnetic catalyst from Suzuki-Miyaura cross-coupling.

BET analysis was performed to confirm the surface functionalization of Fe_3O_4 . Fig. 3 shows the nitrogen adsorption-desorption curve for (a) MNPs, (b) SMNPs, and (c) the $\text{NO}_2\text{-NHC-Pd@Fe}_3\text{O}_4$ nanomagnetic catalyst. The $\text{NO}_2\text{-NHC-Pd@Fe}_3\text{O}_4$ nanomagnetic catalyst exhibited a type-II isotherm. The amount of N_2 adsorbed on bare MNPs was high as compared to SMNPs and the $\text{NO}_2\text{-NHC-Pd@Fe}_3\text{O}_4$ nanomagnetic catalyst. Fe_3O_4 showed a surface area of

77.47 m^2g^{-1} that was reduced to 76.60 m^2g^{-1} after surface functionalization with (3-chloropropyl)triethoxysilane. The surface area further decreased for the $\text{NO}_2\text{-NHC-Pd@Fe}_3\text{O}_4$ nanomagnetic catalyst to 69.61 m^2g^{-1} , which confirms the surface functionalization of Fe_3O_4 .

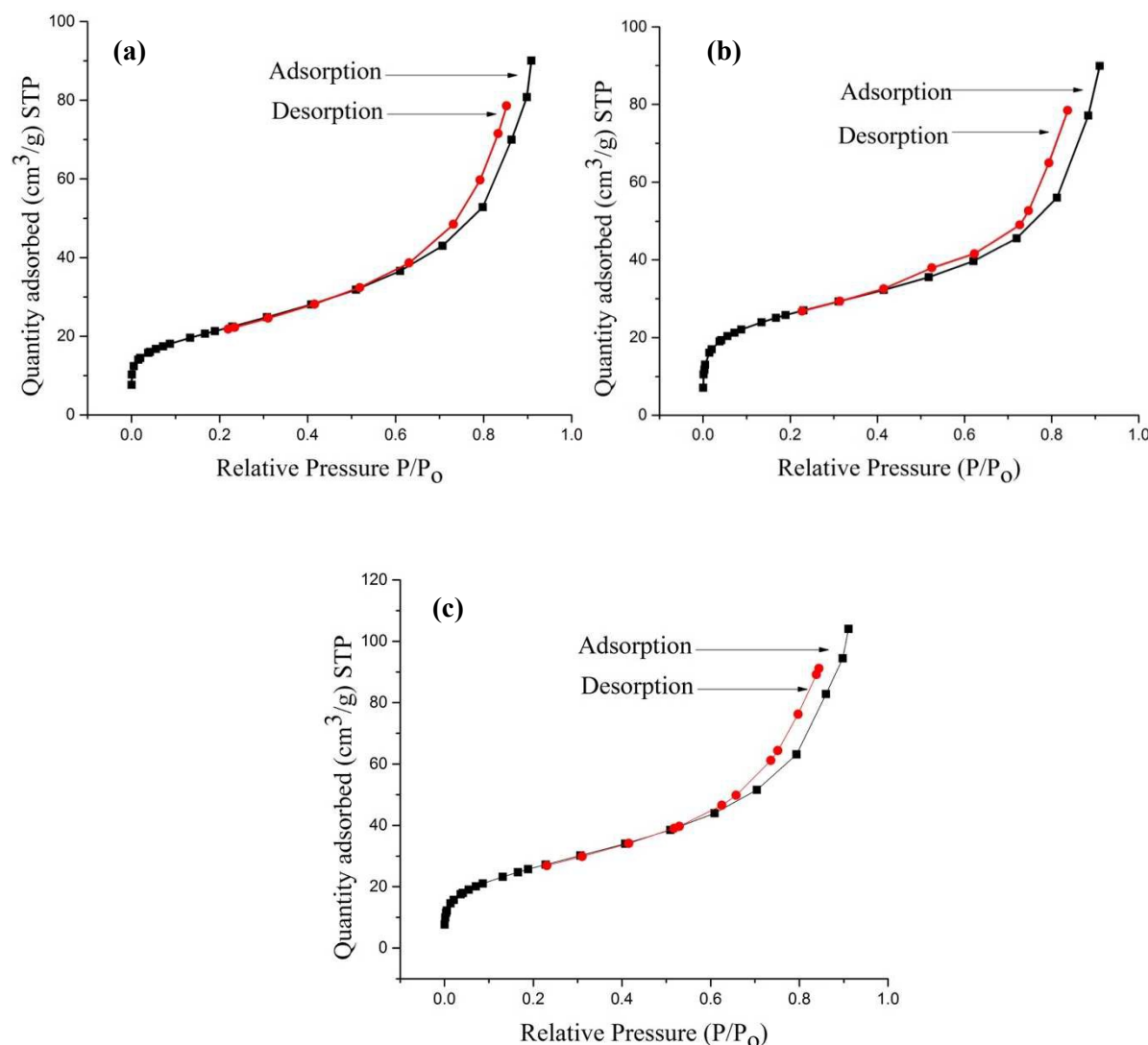


Fig. 3. Nitrogen adsorption-desorption curves for (a) MNPs, (b) SMNPs and (c) $\text{NO}_2\text{-NHC-Pd@Fe}_3\text{O}_4$ nanomagnetic catalyst.

TEM analysis was performed to observe the morphology and size of Fe_3O_4 nanoparticles and the $\text{NO}_2\text{-NHC-Pd@Fe}_3\text{O}_4$ nanomagnetic catalyst (Fig. 4). Quasi-spherical morphology was observed for Fe_3O_4 , with sizes ranging from 7-11 nm. After the grafting of the NHC-

palladium(II) complex, the particle size increased to 11-15 nm with quasi-spherical morphology (Fig. 4b). Due to their relatively high contrast, TEM images show the magnetic core as dark spots inside the quasi-spherical $\text{NO}_2\text{-NHC-Pd@Fe}_3\text{O}_4$ nanomagnetic catalysts. The TEM image of seven times recycled $\text{NO}_2\text{-NHC-Pd@Fe}_3\text{O}_4$ nanomagnetic catalyst from Suzuki-Miyaura cross-coupling (Fig. 4c) shows an almost identical morphology and size.

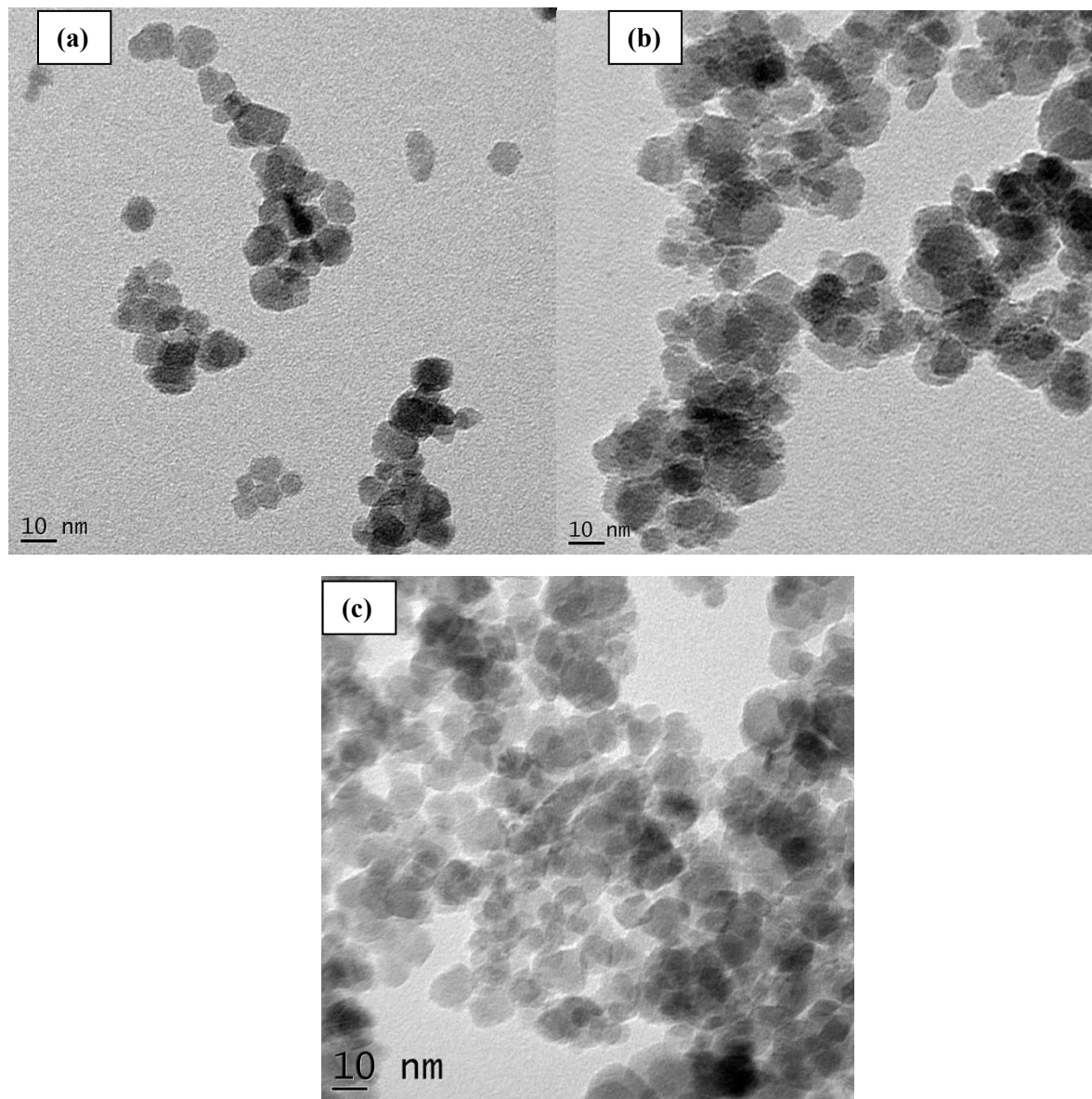


Fig. 4. TEM images of (a) MNPs, (b) NO₂-NHC-Pd@Fe₃O₄ nanomagnetic catalyst and (c) seven times recycled NO₂-NHC-Pd@Fe₃O₄ nanomagnetic catalyst from Suzuki-Miyaura cross-coupling.

The morphology and size of the NO₂-NHC-Pd@Fe₃O₄ nanomagnetic catalyst and the recycled NO₂-NHC-Pd@Fe₃O₄ nanomagnetic catalyst were evaluated through FESEM (Fig. 5). The FESEM image of the NO₂-NHC-Pd@Fe₃O₄ nanomagnetic catalyst shows the formation of uniform nanometer-sized spherical particles (Fig. 5a). Very interestingly, seven times recycled NO₂-NHC-Pd@Fe₃O₄ nanomagnetic catalyst from Suzuki-Miyaura cross-coupling reaction displayed the same morphology and size and which is in good agreement with TEM results. Elemental dot-mapping of the NO₂-NHC-Pd@Fe₃O₄ nanomagnetic catalyst was carried out using EDS (Fig. 6). The characteristic peaks of all the elements present (C, N, O, Fe, Si, Pd and Cl) in the NO₂-NHC-Pd@Fe₃O₄ nanomagnetic catalyst was confirmed by energy-dispersive X-ray spectroscopy EDS (Fig. 7). Thus, EDS spectrum confirms the successful grafting of NHC–palladium(II) complex on Fe₃O₄. All the elements present in the catalyst are uniformly scattered, which is evident from the area mapping by EDS, as shown in Fig. 6. Quantitative assessment of palladium(II) loading in the NO₂-NHC-Pd@Fe₃O₄ nanomagnetic catalyst was determined by ICP-AES. The ICP-AES analysis of the catalyst revealed that 2.48% w/w of palladium was loaded onto the Fe₃O₄ nanomagnetic support.

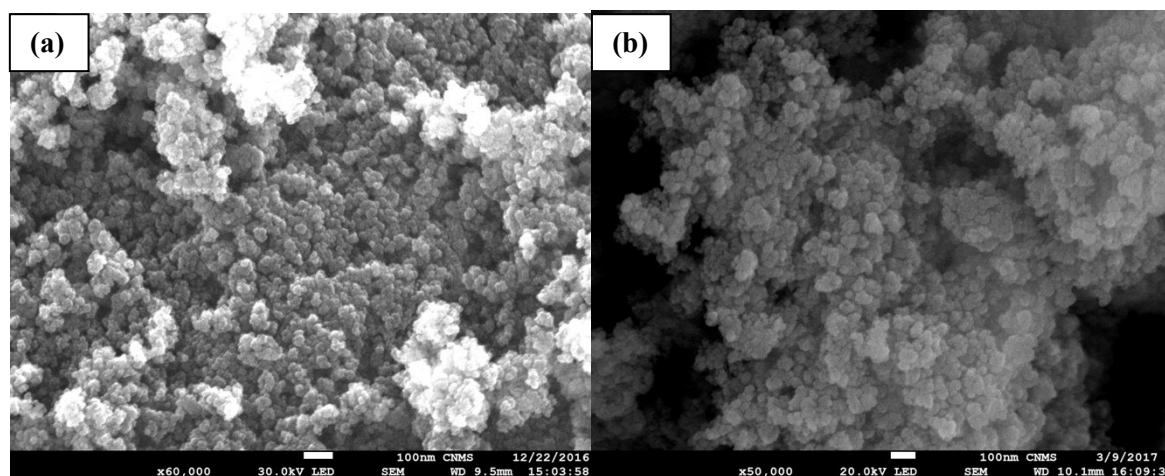
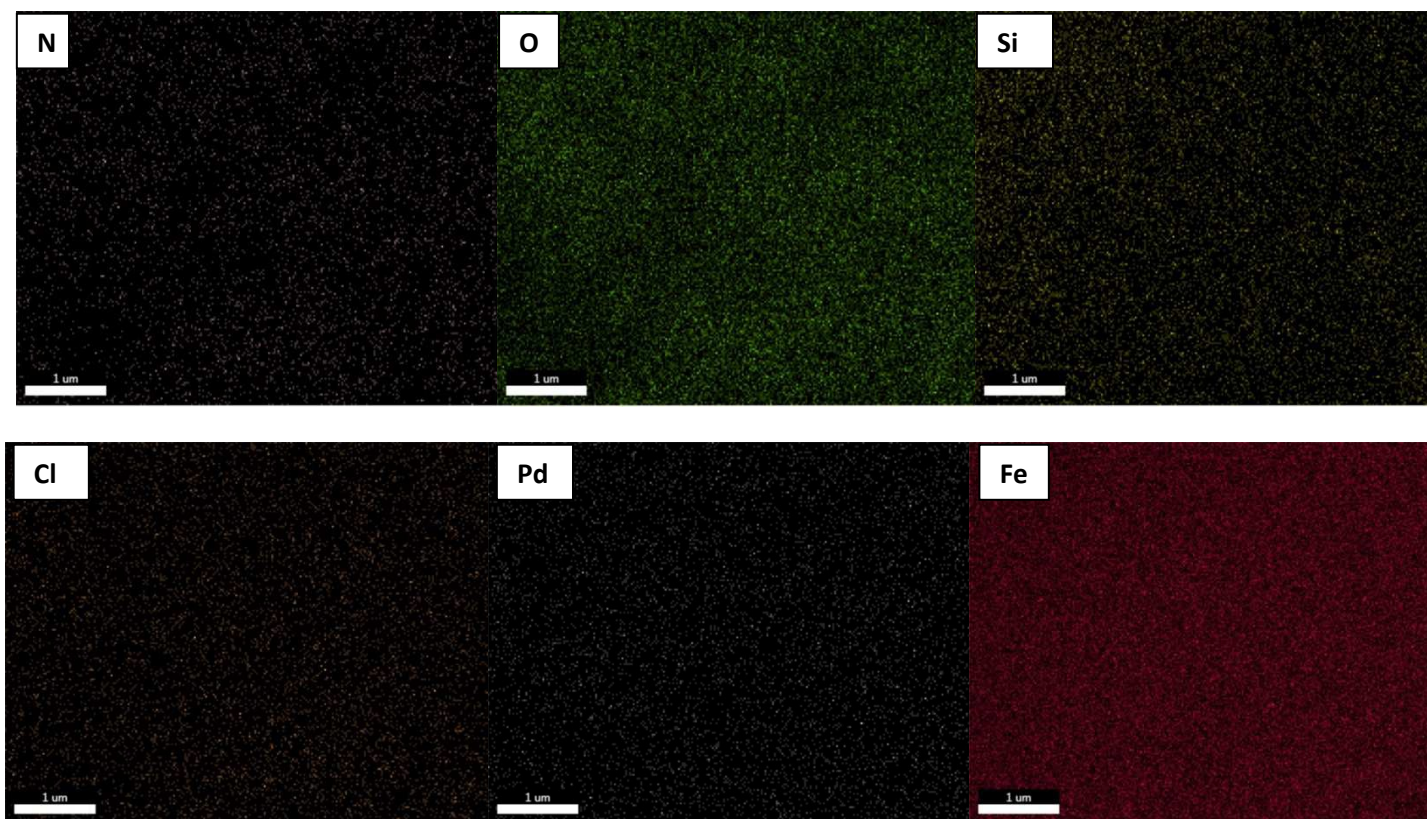


Fig. 5. FESEM images of (a) $\text{NO}_2\text{-NHC-Pd@Fe}_3\text{O}_4$ nanomagnetic catalyst and (b) seven times recycled $\text{NO}_2\text{-NHC-Pd@Fe}_3\text{O}_4$ nanomagnetic catalyst from Suzuki-Miyaura cross-coupling.



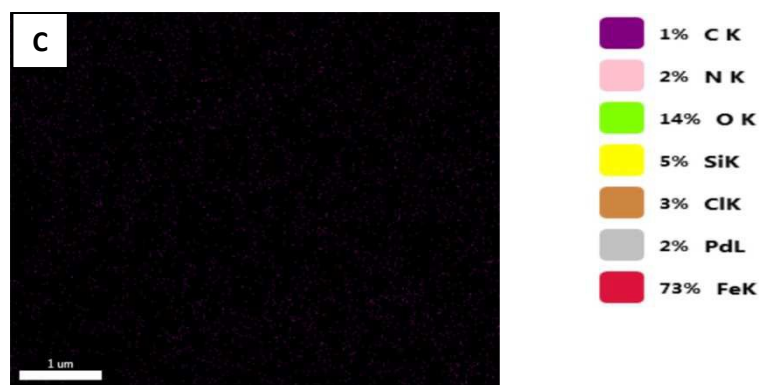


Fig. 6. EDS elemental mapping of the NO₂-NHC-Pd@Fe₃O₄ nanomagnetic catalyst.

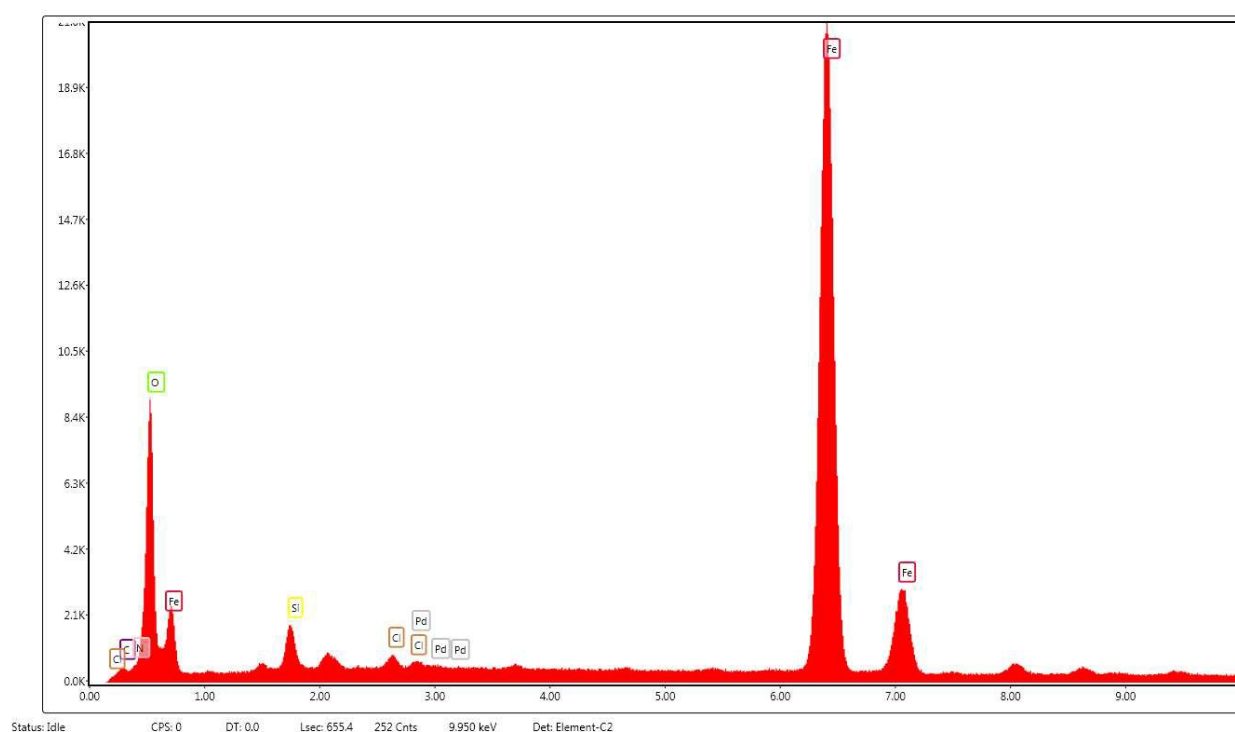


Fig. 7. EDS spectrum of NO₂-NHC-Pd@Fe₃O₄ nanomagnetic catalyst.

The X-ray powder diffraction (XRD) pattern of Fe₃O₄ (Fig. 8a) shows a cubic spinel structure, with peaks attributed to Fe₃O₄ at $2\theta = 30.09^\circ$, 35.59° , 43.07° , 53.43° , 57.37° and 62.90° , which corresponds to the reflection planes (220), (311), (400), (422), (511) and (440), respectively. From the XRD pattern of the NO₂-NHC-Pd@Fe₃O₄ nanomagnetic catalyst (Fig. 8b), it is clear that the phase remained unaltered even after anchoring of the NHC-palladium(II)

complex onto Fe_3O_4 . No characteristic peaks for palladium were detected in the XRD pattern of the nanomagnetic catalyst, which indicates that the palladium sites are well dispersed on the magnetite support.³⁵ The crystal size of Fe_3O_4 , obtained using the Debye Scherrer equation, was 12.85 nm; the $\text{NO}_2\text{-NHC-Pd@Fe}_3\text{O}_4$ nanomagnetic catalyst was 13.52 nm, which is in agreement with TEM images.

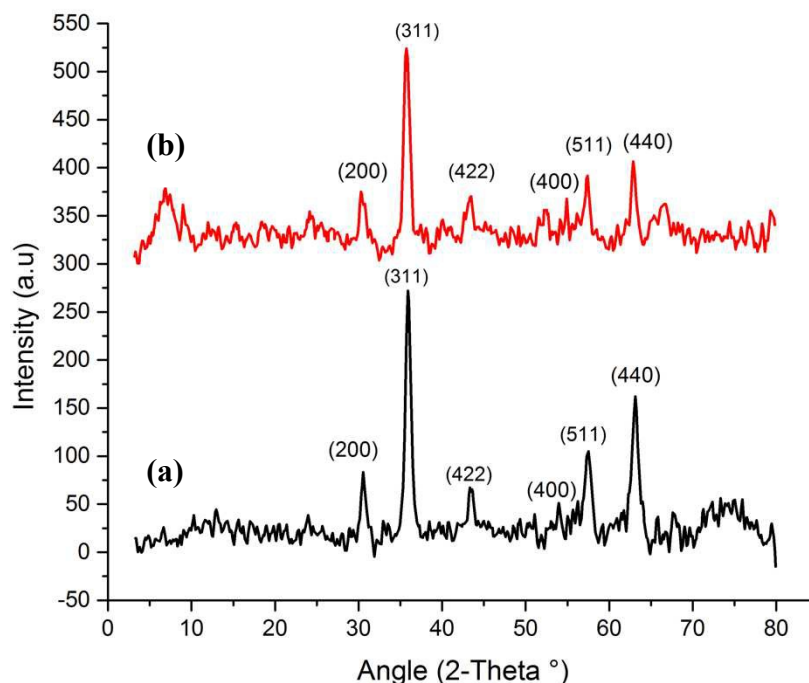


Fig. 8. XRD patterns of (a) MNPs and (b) $\text{NO}_2\text{-NHC-Pd@Fe}_3\text{O}_4$ nanomagnetic catalyst.

Thermogravimetric analysis (TGA) was performed to study the thermal stability of Fe_3O_4 nanoparticles and the $\text{NO}_2\text{-NHC-Pd@Fe}_3\text{O}_4$ nanomagnetic catalyst, using a heating rate of 10 °C/min under a nitrogen atmosphere between 40 °C and 730 °C (Fig. 9). The loss of surface hydroxyl groups and moisture resulted in a weight loss of 6% between 80-200 °C for Fe_3O_4 (Fig. 9a), whereas the $\text{NO}_2\text{-NHC-Pd@Fe}_3\text{O}_4$ nanomagnetic catalyst showed decomposition in two stages (Fig. 9b). The loss of adsorbed water molecules at a temperature up to 110 °C forms the first stage; loss of covalently bonded organic moieties at a temperature up to 500 °C resulted in a

weight loss of 7.8%. Also, it is clear that the $\text{NO}_2\text{-NHC-Pd@Fe}_3\text{O}_4$ nanomagnetic catalyst is stable up to 220-250 °C, which is advantageous for its use in high-temperature reactions.

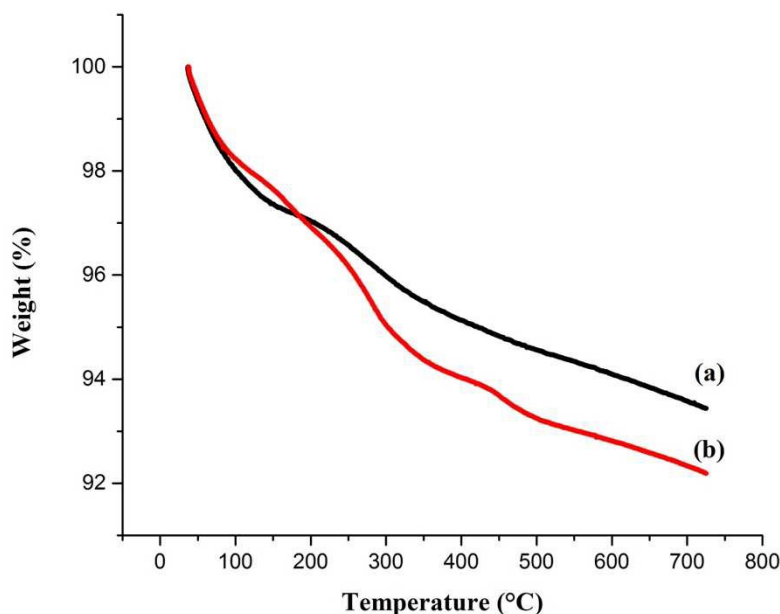


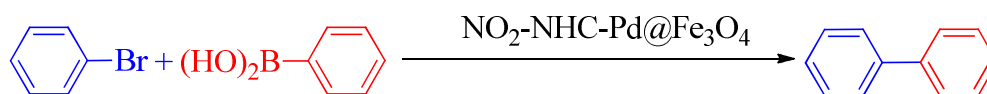
Fig. 9. TGA curve of (a) MNPs and (b) $\text{NO}_2\text{-NHC-Pd@Fe}_3\text{O}_4$ nanomagnetic catalyst.

3.3 Application of the $\text{NO}_2\text{-NHC-Pd@Fe}_3\text{O}_4$ nanomagnetic catalyst in Suzuki-Miyaura cross-coupling reactions

Subsequent to the complete characterization of the $\text{NO}_2\text{-NHC-Pd@Fe}_3\text{O}_4$ nanomagnetic catalyst by a suite of analytical techniques, the catalytic potential of the nanomagnetic catalyst for Suzuki–Miyaura cross-coupling reactions was assessed. The Suzuki–Miyaura cross-coupling reaction between bromobenzene and phenylboronic acid was chosen as the model reaction. Varying sets of conditions were assessed for the Suzuki–Miyaura cross-coupling reaction (Table 1), which resulted yields as high as 95%. We found that increases in time and temperature did not improve the yield, and the optimal catalyst ratio was 0.15 mol% of palladium. Also, the use of potassium carbonate and $\text{EtOH:H}_2\text{O}$ (1:1) was superior relative to the use of other bases and solvents. However, unlike our previously reported nanomagnetic catalyst³³, the reaction

proceeded well at room temperature. The increased steric bulk caused by the nitro group in NHC ligand may be the reason for better activity of the $\text{NO}_2\text{-NHC-Pd@Fe}_3\text{O}_4$ nanomagnetic catalyst at lower temperatures. Thus, through a series of reactions, the Suzuki–Miyaura cross-coupling reaction conditions were optimized with potassium carbonate as base, EtOH:H₂O (1:1) mixture as solvent, room temperature and 0.15 mol% of palladium as the catalyst ratio for 2 h.

Table 1. Optimization of conditions for Suzuki-Miyaura cross-coupling reaction of bromobenzene with phenylboronic acid in the presence of the $\text{NO}_2\text{-NHC-Pd@Fe}_3\text{O}_4$ nanomagnetic catalyst^a.



Entry	Base	Solvent	Temp. (°C)	Pd (mol %)	Time (h)	Yield (%) ^b
1	K ₂ CO ₃	EtOH:H ₂ O (1:1)	70	0.15	1	95
2	K ₂ CO ₃	EtOH:H ₂ O (1:1)	70	0.15	2	95
3	K ₂ CO ₃	EtOH:H ₂ O (1:1)	50	0.15	1	95
4	K ₂ CO ₃	EtOH:H ₂ O (1:1)	R.T	0.15	1	85
5	K₂CO₃	EtOH:H₂O (1:1)	R.T	0.15	2	95
6	K ₂ CO ₃	EtOH:H ₂ O (1:1)	R.T	0.15	3	95
7	K ₂ CO ₃	EtOH:H ₂ O (1:1)	R.T	0.10	2	83
8	K ₂ CO ₃	EtOH:H ₂ O (1:1)	R.T	0.10	3	85
9	K ₂ CO ₃	EtOH:H ₂ O (1:1)	R.T	0.2	1	95
10	K ₂ CO ₃	EtOH:H ₂ O (1:1)	R.T	0.2	2	95
11	Na ₂ CO ₃	EtOH:H ₂ O (1:1)	R.T	0.15	2	80
11	Na ₂ CO ₃	EtOH:H ₂ O (1:1)	R.T	0.15	3	90
12	Na ₃ PO ₄	EtOH:H ₂ O (1:1)	R.T	0.15	3	73
13	CsCO ₃	EtOH:H ₂ O (1:1)	R.T	0.15	3	78
14	K ₂ CO ₃	EtOH	R.T	0.15	3	75
15	K ₂ CO ₃	H ₂ O	R.T	0.15	3	78
16	K ₂ CO ₃	DMF	R.T	0.15	3	58

^aReaction conditions: Bromobenzene (1.0 mmol), phenylboronic acid (1.1 mmol), base (2.2 mmol) and solvent (5 mL) in air.

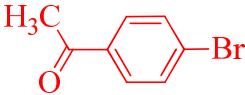
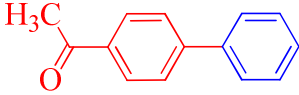
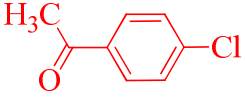
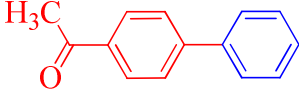
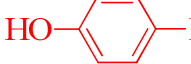
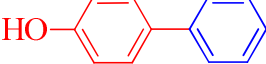
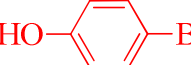
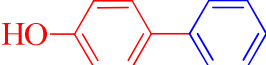

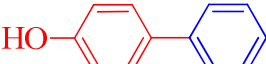
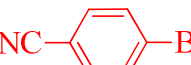
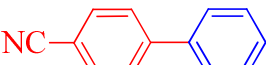
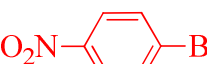
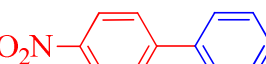
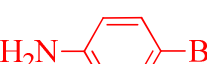
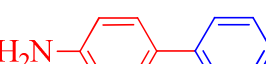
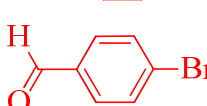
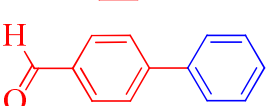
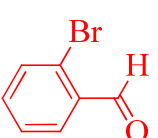
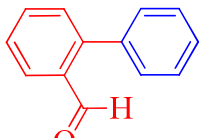
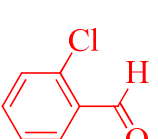
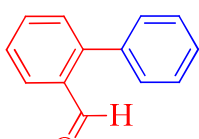
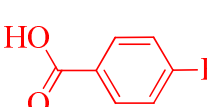
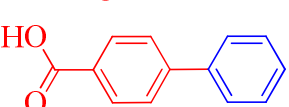
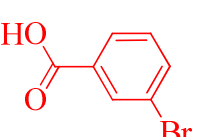
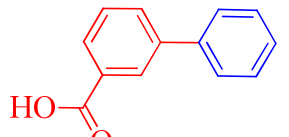
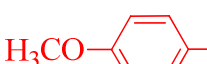

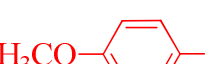

^bIsolated yield after separation by column chromatography; average of two runs.

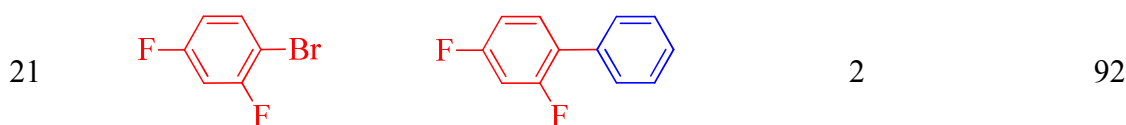
The catalytic activity of the $\text{NO}_2\text{-NHC-Pd@Fe}_3\text{O}_4$ nanomagnetic catalyst was explored in Suzuki-Miyaura cross-coupling between various aryl halides and phenylboronic acid, as shown in Table 2. Among the various aryl halides employed, with both electron-donating groups as well

as electron-withdrawing groups, the $\text{NO}_2\text{-NHC-Pd@Fe}_3\text{O}_4$ nanomagnetic catalyst gave comparable yields under the optimized conditions. It is observed that the steric effect greatly hindered the reaction, and it has been clearly demonstrated by the comparison of the cross-coupling reaction yields of 2-bromobenzaldehyde as well as 4-bromobenzaldehyde with phenylboronic acid. In addition, aryl iodides gave excellent yields when compared to their bromide and chloride counterparts due to the increased reactivity of aryl iodides. Aryl bromides in turn gave good yields when compared with their chloride counterpart. The selectivity of the $\text{NO}_2\text{-NHC-Pd@Fe}_3\text{O}_4$ nanomagnetic catalyst was confirmed by the presence of a negligible amount of homocoupled product obtained. For further authentication on selectivity, Suzuki–Miyaura cross-coupling reactions were carried out without aryl halides under optimized conditions. The biphenyl homocoupled product obtained was in a trace amount, which proved that the $\text{NO}_2\text{-NHC-Pd@Fe}_3\text{O}_4$ nanomagnetic catalyst is highly selective.^{36, 37}

Table 2. Suzuki-Miyaura cross-coupling reactions of different aryl halides with phenylboronic acid by using $\text{NO}_2\text{-NHC-Pd@Fe}_3\text{O}_4$ nanomagnetic catalyst^a.

Entry	Aryl halide	Product	Time (h)	Yield (%) ^b
1			1	98
2			2	95
3			4	89
4			1	90
5			2	84

6			2	95
7			3	80
8			1	93
9			2	86
10			6	52
11			2	94
12			2	96
13			2	91
14			3	85
15			7	57
16			24	-
17			2	90
18			2	91
19			1	99
20			2	93



^aReaction conditions: Aryl halide (1.0 mmol), phenylboronic acid (1.1 mmol), NO₂-NHC-Pd@Fe₃O₄ nanomagnetic catalyst (0.15 mol% Pd with respect to aryl halide), base (2.2 mmol) and solvent (5 mL) in air.

^bIsolated yield after separation by column chromatography; average of two runs.

3.4 Recyclability of the NO₂-NHC-Pd@Fe₃O₄ nanomagnetic catalyst in Suzuki-Miyaura cross-coupling reactions

Recovery and recycling of the catalyst after reaction completion is the key benefit associated with heterogeneous catalysts. In order to study the recycling efficiency of the NO₂-NHC-Pd@Fe₃O₄ nanomagnetic catalyst, the Suzuki–Miyaura cross-coupling reaction between bromobenzene and phenylboronic acid was chosen. From the recycling study as shown in Table 3, the NO₂-NHC-Pd@Fe₃O₄ nanomagnetic catalyst retained its activity up to seven recycles without a considerable drop (Fig. 10). From the eighth-cycle onwards, a drop in yield is observed which reached up to 81% by the end of the eleventh recycle. The reaction conditions employed were milder when compared to our previous work³³, which may also account for the increase in number of recycles.

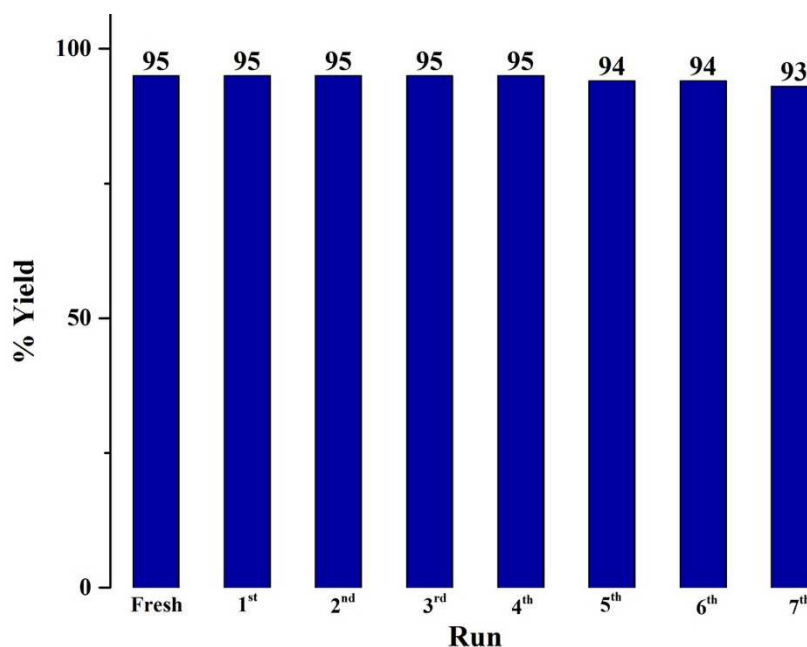


Fig. 10. Recycling efficiency of the NO₂-NHC-Pd@Fe₃O₄ nanomagnetic catalyst for the reaction of bromobenzene and phenylboronic acid.

Table 3. Recyclability of NO₂-NHC-Pd@Fe₃O₄ nanomagnetic catalyst in Suzuki-Miyaura cross-coupling reactions of bromobenzene with phenylboronic acid^a.

Entry	Base	Solvent	Temp. (°C)	Catalyst run	Yield (%) ^b
1	K ₂ CO ₃	EtOH:H ₂ O (1:1)	R.T	Fresh	95
2	K ₂ CO ₃	EtOH:H ₂ O (1:1)	R.T	1 st recycle	95
3	K ₂ CO ₃	EtOH:H ₂ O (1:1)	R.T	2 nd recycle	95
4	K ₂ CO ₃	EtOH:H ₂ O (1:1)	R.T	3 rd recycle	95
5	K ₂ CO ₃	EtOH:H ₂ O (1:1)	R.T	4 th recycle	95
6	K ₂ CO ₃	EtOH:H ₂ O (1:1)	R.T	5 th recycle	94
7	K ₂ CO ₃	EtOH:H ₂ O (1:1)	R.T	6 th recycle	94
8	K ₂ CO ₃	EtOH:H ₂ O (1:1)	R.T	7 th recycle	93
9	K ₂ CO ₃	EtOH:H ₂ O (1:1)	R.T	8 th recycle	90
10	K ₂ CO ₃	EtOH:H ₂ O (1:1)	R.T	9 th recycle	87
11	K ₂ CO ₃	EtOH:H ₂ O (1:1)	R.T	10 th recycle	83
12	K ₂ CO ₃	EtOH:H ₂ O (1:1)	R.T	11 th recycle	81

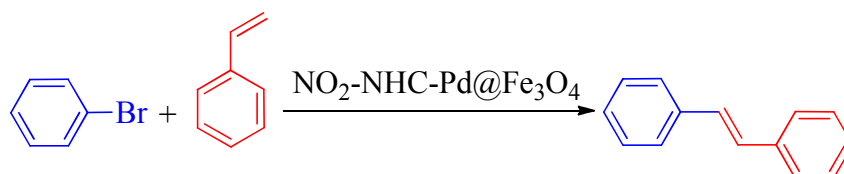
^aReaction conditions: Bromobenzene (1.0 mmol), phenylboronic acid (1.1 mmol), NO₂-NHC-Pd@Fe₃O₄ nanomagnetic catalyst (0.15 mol% Pd with respect to aryl halide), base (2.2 mmol) and solvent (5 mL) in air.

^bIsolated yield after separation by column chromatography; average of two runs.

3.5 Application of the $\text{NO}_2\text{-NHC-Pd@Fe}_3\text{O}_4$ nanomagnetic catalyst in Mizoroki-Heck cross-coupling reactions

Encouraged by the excellent results obtained from Suzuki–Miyaura cross-coupling reactions, we proceeded to study the catalytic activity of $\text{NO}_2\text{-NHC-Pd@Fe}_3\text{O}_4$ nanomagnetic catalyst in Mizoroki–Heck cross-coupling reactions. The cross-coupling reaction between bromobenzene and styrene was taken as the model reaction. The reaction conditions were optimized by following a series of reactions, as listed in Table 4. Reactions were carried out by varying different parameters such as base, solvent, temperature, and catalyst ratio to determine the optimum conditions. Among the bases used for the reaction, sodium phosphate dodecahydrate was found superior. Regarding solvents, acetonitrile (MeCN) was found promising at a temperature of 80 °C, followed by 6 h reaction time with 1 mol% of palladium catalyst.

Table 4. Optimization of conditions for the Mizoroki-Heck cross-coupling reaction of bromobenzene with styrene in the presence of $\text{NO}_2\text{-NHC-Pd@Fe}_3\text{O}_4$ nanomagnetic catalyst^a.



Entry	Base	Solvent	Temp. (°C)	Pd (mol %)	Time (h)	Yield (%) ^b
1	K_2CO_3	EtOH:H ₂ O (1:1)	R.T	0.15	6	10
2	K_2CO_3	EtOH:H ₂ O (1:1)	50°C	0.15	6	23
3	K_2CO_3	EtOH:H ₂ O (1:1)	70°C	0.15	6	50
4	K_2CO_3	EtOH:H ₂ O (1:1)	70°C	0.25	6	60
5	K_2CO_3	EtOH:H ₂ O (1:1)	70°C	0.5	6	75
6	K_2CO_3	EtOH:H ₂ O (1:1)	70°C	1	6	78
7	$\text{Na}_3\text{PO}_4 \cdot 12\text{H}_2\text{O}$	EtOH:H ₂ O (1:1)	70°C	1	6	85
8	$\text{Na}_3\text{PO}_4 \cdot 12\text{H}_2\text{O}$	EtOH:H ₂ O (1:1)	80°C	1	6	88
9	$\text{Na}_3\text{PO}_4 \cdot 12\text{H}_2\text{O}$	EtOH:H ₂ O (1:1)	100°C	1	6	90
10	$\text{Na}_3\text{PO}_4 \cdot 12\text{H}_2\text{O}$	MeCN	80°C	1	6	92
11	$\text{Na}_3\text{PO}_4 \cdot 12\text{H}_2\text{O}$	MeCN	80°C	2	6	92
12	$\text{Na}_3\text{PO}_4 \cdot 12\text{H}_2\text{O}$	MeCN	80°C	1	12	92

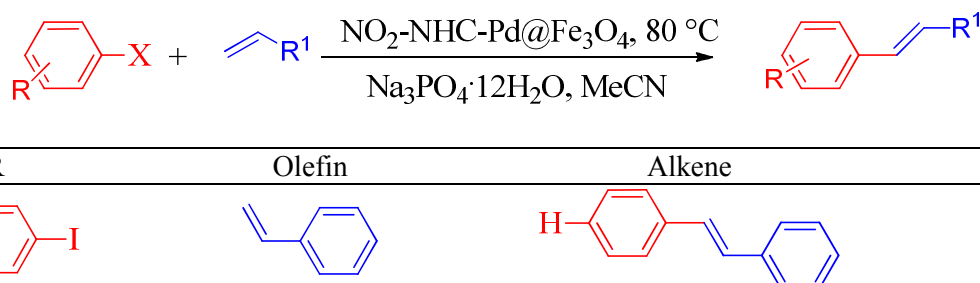
13	Na ₃ PO ₄ ·12H ₂ O	MeCN	80°C	1	3	81
14	Na ₃ PO ₄ ·12H ₂ O	MeCN	R.T	1	6	50
15	Na ₃ PO ₄ ·12H ₂ O	1,4-Dioxane	80°C	1	6	55
16	Na ₃ PO ₄ ·12H ₂ O	Acetone	56°C	1	6	25
17	Na ₃ PO ₄ ·12H ₂ O	Toluene	80°C	1	6	70
18	Na ₃ PO ₄ ·12H ₂ O	DMF	80°C	1	6	83
19	Na ₃ PO ₄ ·12H ₂ O	EtOH	78°C	1	6	48
20	Na ₃ PO ₄ ·12H ₂ O	H ₂ O	80°C	1	6	39
21	NaOH	MeCN	80°C	1	6	28
22	Na ₂ CO ₃	MeCN	80°C	1	6	68
23	CsCO ₃	MeCN	80°C	1	6	72

^aReaction conditions: bromobenzene (1.0 mmol), styrene (1.2 mmol), NO₂-NHC-Pd@Fe₃O₄ nanomagnetic catalyst (1 mol% Pd with respect to aryl halide), base (2.0 mmol) and solvent (5 mL) in air.

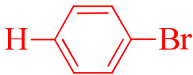
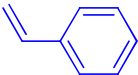
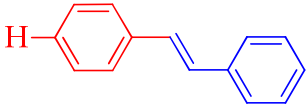
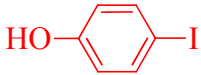
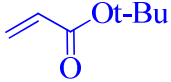
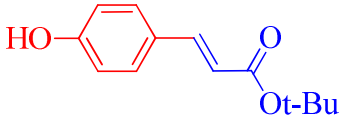
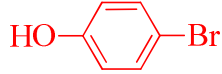
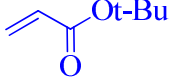
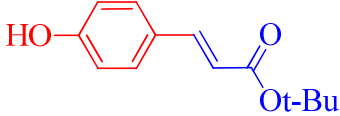
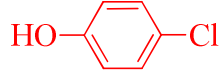
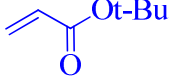
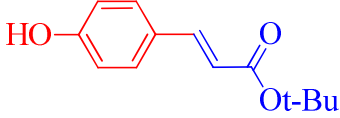
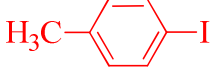
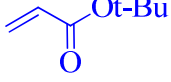
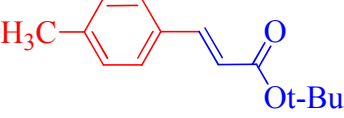
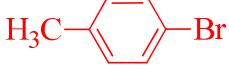
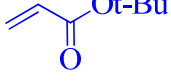
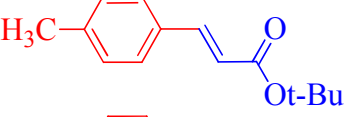
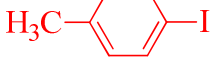
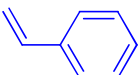
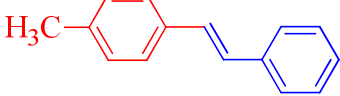
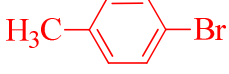
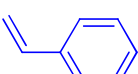
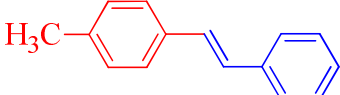
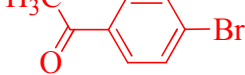
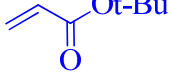
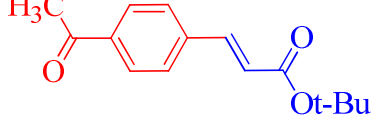
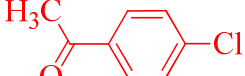
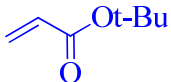
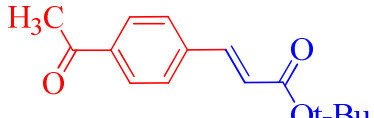
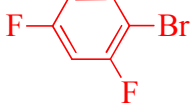
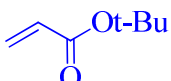
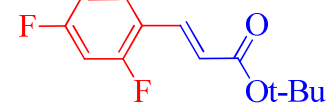
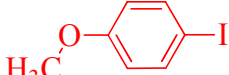
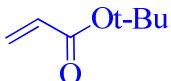
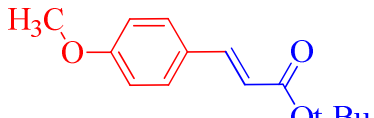
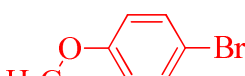
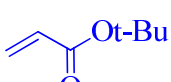
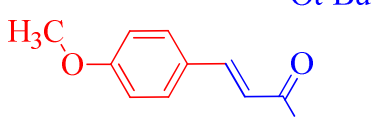
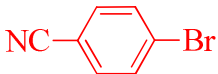
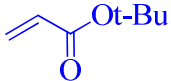
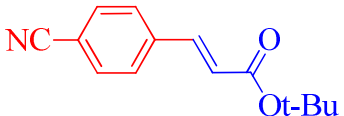
^bIsolated yield after separation by column chromatography; average of two runs.

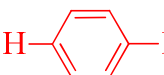
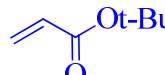
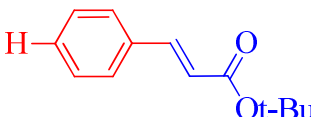
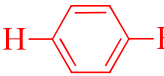
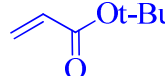
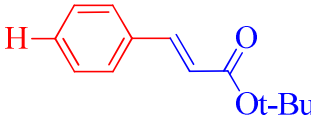
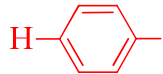
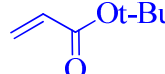
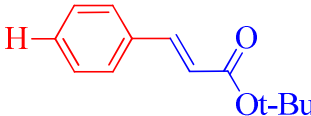
In order to examine the scope of the NO₂-NHC-Pd@Fe₃O₄ nanomagnetic catalyst in arylation of olefins, various aryl halides were coupled with alkenes under the optimized conditions, as shown in Table 5. Due to increased reactivity of aryl iodides, coupling was faster and resulted in excellent yields. Aryl bromides also reacted efficiently with alkenes under optimized conditions resulting in good yields. But aryl chlorides gave lower yields when compared to their iodide and bromide counterparts. On the other hand, aryl halides with both electron-donating groups and electron-withdrawing groups were well tolerated and gave desired cross-coupling products in good to excellent yields in different time duration.³⁸ From these results, it can be concluded that the NO₂-NHC-Pd@Fe₃O₄ nanomagnetic catalyst can catalyze Mizoroki–Heck cross-coupling reaction efficiently.

Table 5. Mizoroki–Heck cross-coupling of different aryl halides with alkenes in the presence of NO₂-NHC-Pd@Fe₃O₄ nanomagnetic catalyst^a.



Entry	R	Olefin	Alkene	Time (h)	Yield (%) ^b
1				5	96

2				6	92
3				6	95
4				6	90
5				9	75
6				6	90
7				8	85
8				6	89
9				9	86
10				8	84
11				12	58
12				7	84
13				8	90
14				10	82
15				8	78

16				4	96
17				6	93
18				12	66

^aReaction conditions: Aryl halide (1.0 mmol), alkene (1.2 mmol), NO₂-NHC-Pd@Fe₃O₄ nanomagnetic catalyst (1 mol% Pd with respect to aryl halide), base (2.0 mmol) and solvent (5 mL) in air.

^bIsolated yield after separation by column chromatography; average of two runs.

3.6 Recyclability of the NO₂-NHC-Pd@Fe₃O₄ nanomagnetic catalyst in Mizoroki-Heck cross-coupling reactions

The recyclability of the NO₂-NHC-Pd@Fe₃O₄ nanomagnetic catalyst in Mizoroki-Heck cross-coupling was also studied for the model reaction under optimized conditions, which is shown in Table 6. From the results obtained, it can be concluded that there is no significant loss in activity of the NO₂-NHC-Pd@Fe₃O₄ nanomagnetic catalyst for up to five recycles (Fig. 11). However, further recycles resulted in decreases in the yield of the cross-coupled product, still resulting in a respectable yield of 74% after 12 recycles. Recycling efficiency has been reduced in the case of Mizoroki-Heck cross-coupling when compared to that of Suzuki-Miyaura cross-coupling reaction. The difference in reaction conditions employed may be one of the key reasons for this. The Suzuki-Miyaura cross-coupling is carried out at room temperature whereas Mizoroki-Heck cross-coupling is carried out at 80 °C. This may facilitate a gradual decay of the NO₂-NHC-Pd@Fe₃O₄ nanomagnetic catalyst. Also, acetonitrile solvent may coordinate with the palladium during the reaction resulting in slow catalyst poisoning.³⁹

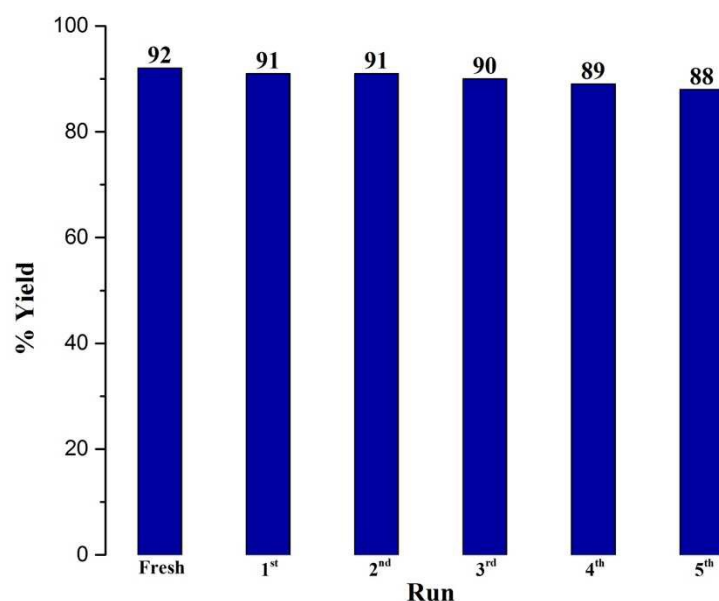


Fig. 11. Recycling efficiency of the NO₂-NHC-Pd@Fe₃O₄ nanomagnetic catalyst in the reaction of bromobenzene and styrene.

Table 6. Recyclability of the NO₂-NHC-Pd@Fe₃O₄ nanomagnetic catalyst in Mizoroki–Heck cross-coupling reactions of bromobenzene with styrene^a.

Entry	Base	Solvent	Temp. (°C)	Catalyst Run	Yield (%) ^b
1	Na ₃ PO ₄ ·12H ₂ O	MeCN	80°C	Fresh	92
2	Na ₃ PO ₄ ·12H ₂ O	MeCN	80°C	1 st recycle	91
3	Na ₃ PO ₄ ·12H ₂ O	MeCN	80°C	2 nd recycle	91
4	Na ₃ PO ₄ ·12H ₂ O	MeCN	80°C	3 rd recycle	90
5	Na ₃ PO ₄ ·12H ₂ O	MeCN	80°C	4 th recycle	89
6	Na ₃ PO ₄ ·12H ₂ O	MeCN	80°C	5 th recycle	88
7	Na ₃ PO ₄ ·12H ₂ O	MeCN	80°C	6 th recycle	81
12	Na ₃ PO ₄ ·12H ₂ O	MeCN	80°C	7 th recycle	74

^aReaction conditions: Aryl halide (1.0 mmol), alkene (1.2 mmol), NO₂-NHC-Pd@Fe₃O₄ nanomagnetic catalyst (1 mol% Pd with respect to aryl halide), base (2.0 mmol) and solvent (5 mL) in air.

^bIsolated yield after separation by column chromatography; average of two runs.

3.7 Catalyst leaching study

From ATR-IR (Fig. 2d), TEM (Fig. 4c) and FESEM (Fig. 5b) analysis, it is very clear that the seven times recycled NO₂-NHC-Pd@Fe₃O₄ nanomagnetic catalyst from Suzuki-Miyaura cross-coupling reaction has retained its structure and morphology. Even though there are some

shifts of peaks in IR spectrum for the recycled NO₂-NHC-Pd@Fe₃O₄ nanomagnetic catalyst, there is no marked change observed after seven recycles. Also both TEM and FESEM results confirm the detainment of morphology of NO₂-NHC-Pd@Fe₃O₄ nanomagnetic catalyst after seven recycles in Suzuki-Miyaura cross-coupling. Further, to confirm the heterogeneity and to understand the leaching of the NO₂-NHC-Pd@Fe₃O₄ nanomagnetic catalyst during Suzuki-Miyaura cross-coupling between bromobenzene and phenylboronic acid, the NO₂-NHC-Pd@Fe₃O₄ nanomagnetic catalyst was separated by magnetic decantation quickly from the reaction mass after 30 minutes and the reaction was allowed to continue for further 2 h which resulted in 55% isolated yield of cross-coupled product. At the same time, another reaction between the same reactants under identical conditions was carried out for 30 minutes followed by workup and isolation of cross-coupled product to afford 50% yield. This confirms that after removal of NO₂-NHC-Pd@Fe₃O₄ nanomagnetic catalyst from the reaction mass, reaction did not proceed further and hence proves that the NO₂-NHC-Pd@Fe₃O₄ nanomagnetic catalyst is heterogeneous in nature.

3.8 Comparison of catalytic activity

In order to understand the distinctiveness of the NO₂-NHC-Pd@Fe₃O₄ nanomagnetic catalyst, we compared the results of Suzuki–Miyaura and Mizoroki–Heck cross-coupling reaction of the catalyst with other supported heterogeneous catalysts, which is given in Table 7 and Table 8, respectively. From the comparison study, it is clear that the NO₂-NHC-Pd@Fe₃O₄ nanomagnetic catalyst shows a better activity in less time and milder reaction conditions for both Suzuki–Miyaura and Mizoroki–Heck cross-coupling reactions. Facile recovery of the NO₂-NHC-Pd@Fe₃O₄ nanomagnetic catalyst, mild reaction conditions, better activity, and excellent

selectivity are the key advantages of the NO₂-NHC-Pd@Fe₃O₄ nanomagnetic catalyst over other reported catalysts.^{33, 36-38, 40-46}

Table 7. Comparison of results for the NO₂-NHC-Pd@Fe₃O₄ nanomagnetic catalyst with other catalysts in the Suzuki-Miyaura cross-coupling reaction between bromobenzene and phenylboronic acid.

Entry	Catalyst	Solvent	Temp. (°C)	Time (h)	Yield (%)	Ref.
1 ^a	Iron oxide-Pd complex	DMF	50	12	77	43
2	MNPs-NHC-Pd(II)	EtOH:H ₂ O (1:1)	R.T	1	93	41
3	NHC-Pd Complex	DMF:H ₂ O (1:1)	50	6	95	38
4 ^a	Catalyst-1	EtOH:H ₂ O (3:1)	70	12	87	36
5	Pd-IL-NH ₂ /SiO ₂ /Fe ₃ O ₄	EtOH:H ₂ O (1:1)	80	5	87	37
6	NHC-Pd@MNPs	EtOH:H ₂ O (1:1)	70	1	95	33
7 ^b	PdNPs	DMF:H ₂ O (1:1)	120	0.17	97	46
8	NO ₂ -NHC-Pd@Fe ₃ O ₄	EtOH:H ₂ O (1:1)	R.T	2	95	Present work
9 ^a	NO ₂ -NHC-Pd@Fe ₃ O ₄	EtOH:H ₂ O (1:1)	R.T	2	93	Present work

^a Coupling reaction between 4-bromoanisole and phenyl boronic acid.

^b Coupling reaction between 4-iodotoluene and phenyl boronic acid.

Table 8. Comparison of results for the NO₂-NHC-Pd@Fe₃O₄Fe₃O₄ nanomagnetic catalyst with other catalysts in the Mizoroki-Heck cross-coupling reaction between bromobenzene and styrene.

Entry	Catalyst	Solvent	Temp. (°C)	Time (h)	Yield (%)	Ref.
1	MNPs-NHC-Pd(II)	DMF	70	0.33	87	41
2	SPIONs-bis(NHC)-palladium(II) diacetate	DMF	90	7	82	42
3 ^a	SiO ₂ @Fe ₃ O ₄ -Pd	DMF	100	8	95	40
4 ^a	Catalyst	DMF	90	24	100	45
5 ^a	MNP@NHC-Pd	DMF	140	-	96	44
6	NO ₂ -NHC-Pd@Fe ₃ O ₄	MeCN	80	6	92	Present work
7 ^a	NO ₂ -NHC-Pd@Fe ₃ O ₄	MeCN	80	5	96	Present work

^a Cross-coupling reaction between iodobenzene and styrene.

4. Conclusion

In summary, we report here a new $\text{NO}_2\text{-NHC-Pd@Fe}_3\text{O}_4\text{Fe}_3\text{O}_4$ nanomagnetic catalyst, synthesized by facile methods under aerobic conditions starting from inexpensive chemicals that are available easily in the market and characterized by various analytical techniques like ATR-IR, ICP-AES, EDS, FESEM, TEM, XRD, TGA, and BET surface area analysis. The catalyst displayed excellent catalytic activity under mild reaction conditions, and was easily recovered after reaction completion with an external magnet, which could be reused several times without a significant loss in activity. Furthermore, magnetite-supported *N*-heterocyclic carbene metal complexes with varying electronic properties which are fine-tuned for improved catalytic activity can be synthesized following this protocol and studied for their catalytic activity in various cross-coupling reactions.

Disclosure of Interest

The authors declared that they have no conflict of interests concerning this article.

Acknowledgements

The authors thank Nano Mission, Ministry of Science & Technology, Department of Science & Technology, Government of India, for financial support through the Grant SR/NM/NS-20/2014.

References

1. S. Kotha, K. Lahiri and D. Kashinath, *Tetrahedron*, 2002, **58**, 9633-9695.
2. A. N. Cammidge and K. V. L. Crépy, *J Org Chem*, 2003, **68**, 6832-6835.
3. N. Miyaura, T. Yanagi and A. Suzuki, *Synth Commun*, 1981, **11**, 513-519.
4. N. Miyaura, K. Yamada and A. Suzuki, *Tetrahedron Lett*, 1979, **20**, 3437-3440.
5. A. J. Lennox and G. C. Lloyd-Jones, *Chem Soc Rev*, 2014, **43**, 412-443.
6. J. P. Knowles and A. Whiting, *Org Biomol Chem*, 2007, **5**, 31-44.

7. C. Torborg and M. Beller, *Adv Synth Catal*, 2009, **351**, 3027-3043.
8. L. Yin and J. Liebscher, *Chem Rev*, 2007, **107**, 133-173.
9. S. Cacchi and G. Fabrizi, *Chem Rev*, 2005, **105**, 2873-2920.
10. P. Anastas and N. Eghbali, *Chem Soc Rev*, 2010, **39**, 301-312.
11. F. Rajabi, D. Schaffner, S. Follmann, C. Wilhelm, S. Ernst and W. R. Thiel, *ChemCatChem*, 2015, **7**, 3513-3518.
12. A. Schatz, T. R. Long, R. N. Grass, W. J. Stark, P. R. Hanson and O. Reiser, *Adv Funct Mater*, 2010, **20**, 4323-4328.
13. V. Polshettiwar, R. Luque, A. Fihri, H. Zhu, M. Bouhrara and J. M. Basset, *Chem Rev*, 2011, **111**, 3036-3075.
14. G. Chouhan, D. Wang and H. Alper, *Chem Commun*, 2007, DOI: 10.1039/b711298j, 4809-4811.
15. N. T. S. Phan and C. W. Jones, *J Mol Catal A: Chem*, 2006, **253**, 123-131.
16. T.-J. Yoon, W. Lee, Y.-S. Oh and J.-K. Lee, *New J Chem*, 2003, **27**, 227-229.
17. A. Aranyos, D. W. Old, A. Kiyomori, J. P. Wolfe, J. P. Sadighi and S. L. Buchwald, *J Am Chem Soc*, 1999, **121**, 4369-4378.
18. L.-C. Liang, *Coordination Chemistry Reviews*, 2006, **250**, 1152-1177.
19. G. R. Peh, E. A. Kantchev, C. Zhang and J. Y. Ying, *Org Biomol Chem*, 2009, **7**, 2110-2119.
20. A. J. Arduengo, R. L. Harlow and M. Kline, *J Am Chem Soc*, 1991, **113**, 361-363.
21. C. M. Crudden and D. P. Allen, *Coord Chem Rev*, 2004, **248**, 2247-2273.
22. M. N. Hopkinson, C. Richter, M. Schedler and F. Glorius, *Nature*, 2014, **510**, 485-496.

23. E. C. Hurst, K. Wilson, I. J. S. Fairlamb and V. Chechik, *New J Chem*, 2009, **33**, 1837-1840.
24. K. V. S. Ranganath, S. Onitsuka, A. K. Kumar and J. Inanaga, *Catal Sci Tech*, 2013, **3**, 2161-2181.
25. M. Ghiaci, M. Zarghani, A. Khojastehnezhad and F. Moeinpour, *RSC Adv*, 2014, **4**, 15496-15501.
26. K. Yavuz and H. Küçükbay, *Appl Organometal Chem*, 2017, DOI: 10.1002/aoc.3897, e3897.
27. H. Küçükbay, Ü. Yilmaz, K. Yavuz and N. Buğday, *Turk J Chem*, 2015, **39**, 1265-1278.
28. W. A. Herrmann and C. Köcher, *Angew Chem Int Ed Engl*, 1997, **36**, 2162-2187.
29. M. Alcarazo, T. Stork, A. Anoop, W. Thiel and A. Furstner, *Angew Chem Int Ed Engl*, 2010, **49**, 2542-2546.
30. S. Díez-González, N. Marion and S. P. Nolan, *Chem Rev*, 2009, **109**, 3612-3676.
31. G. Buscemi, M. Basato, A. Biffis, A. Gennaro, A. A. Isse, M. M. Natile and C. Tubaro, *J Organomet Chem*, 2010, **695**, 2359-2365.
32. W. Wang, F. Wang and M. Shi, *Organometallics*, 2010, **29**, 928-933.
33. K. Vishal, B. D. Fahlman, B. S. Sasidhar, S. A. Patil and S. A. Patil, *Catal Lett*, 2017, **147**, 900-918.
34. H. Küçükbay, R. Durmaz, M. Güven and S. Günal, *Arzneim Forsch*, 2001, **51**, 420-424.
35. V. Polshettiwar and R. S. Varma, *Org Biomol Chem*, 2009, **7**, 37-40.
36. Z. Wang, Y. Yu, Y. Zhang, S. Z. Li, H. Qian and Z. Lin, *Green Chem*, 2015, **17**, 413-420.
37. J. Wang, B. Xu, H. Sun and G. Song, *Tetrahedron Lett*, 2013, **54**, 238-241.

38. J.-H. Kim, J.-W. Kim, M. Shokouhimehr and Y.-S. Lee, *J Org Chem*, 2005, **70**, 6714-6720.
39. B. B. Wayland and R. F. Schramm, *Inorg Chem*, 1969, **8**, 971-976.
40. P. Li, L. Wang, L. Zhang and G.-W. Wang, *Adv Synth Catal*, 2012, **354**, 1307-1318.
41. Hajipour AR, Tadayoni NS and K. Z, *Appl Organometal Chem*, 2016, **30**, 590-595.
42. M. Ghotbinejad, A. R. Khosropour, I. Mohammadpoor-Baltork, M. Moghadam, S. Tangestaninejad and V. Mirkhani, *J Mol Catal A: Chem* 2014, **385**, 78-84.
43. Stevens PD, Fan J, Gardimalla HMR, Yen M and G. Y, *Org Lett*, 2005, **7**, 2085-2088.
44. A. Z. Wilczewska and I. Misztalewska, *Organometallics*, 2014, **33**, 5203-5208.
45. B. Altava, M. I. Burguete, E. García-Verdugo, N. Karbass, S. V. Luis, A. Puzary and V. Sans, *Tetrahedron Lett*, 2006, **47**, 2311-2314.
46. Ü. Yilmaz, H. Küçükbay, S. Türktekin Çelikesir, M. Akkurt and O. Büyükgüngör, *Turk J Chem*, 2013, **37**, 721-733.

Table of Contents

A Convenient, Efficient and Reusable N-Heterocyclic Carbene–Palladium(II) Based Catalyst Supported on Magnetite for Suzuki–Miyaura and Mizoroki–Heck Cross-Coupling Reactions

Vishal Kandathil,^a Bradley D. Fahlman,^b Sasidhar B. S.,^c Shivaputra A. Patil,^d Siddappa A. Patil^{a*}

